Marine and Petroleum Geology 171 (2025) 107210

Contents lists available at ScienceDirect

Marine and Petroleum Geology

journal homepage: www.elsevier.com/locate/marpetgeo

Combined use of petroleum inclusion analysis, PVT simulation, and basin modeling for reconstruction of deep fluid phase evolution in condensate gas reservoirs

Wenzhi Lei [a,b], Dongxia Chen [a,b,*], Ming Cheng [c], Chenyang Cai [a,b], Qiaochu Wang [a,b]

[a] State Key Laboratory of Petroleum Resources and Engineering, China University of Petroleum (Beijing), Beijing, 102249, China
[b] College of Geosciences, China University of Petroleum, Beijing, 102200, China
[c] PetroChina Changqing Oilfield Company, Changbei Operation Company, Xi'an, 710018, China

ARTICLE INFO

Keywords:
Condensate gas reservoir
Deep fluid phase evolution
Petroleum inclusion thermodynamics
PVT simulation
Basin modeling

ABSTRACT

The reconstruction of the fluid phase evolution in deep condensate gas reservoirs can reveal the mechanism of condensate gas formation, facilitating the early formulation of drilling strategies. However, the complexity of petroleum fluid phase evolution during hydrocarbon generation, migration, and accumulation poses numerous challenges for the reconstruction process. Therefore, petroleum fluid inclusion analysis, PVT phase simulation, and basin modeling were used to achieve the reconstruction of phase states during key geological periods, elucidating the phase evolution of the deep condensate reservoirs in the Dongying Depression during the whole process. The modeled results show that the mature source rocks contributed to the charging and accumulation of liquid oils (38–14 Ma). Next, a low oil cracking conversion rate limited the increase of gaseous hydrocarbon fraction, so the accumulated hydrocarbons remained in a liquid phase (14–0 Ma). The late external gas inputs significantly increased the gas-oil ratio in the reservoirs, leading to the transition from the liquid oil phase to the condensate phase (5–0 Ma). The fluid compositions obtained from hydrocarbon inclusions and the physical properties of present-day condensates can effectively constrain basin modeling, leading to reliable simulation results. This work revealed that the hydrocarbon generation controls the initial hydrocarbon components in the traps for the phase evolution. Furthermore, the secondary alterations including oil cracking and gas inputs influence the proportion of methane of petroleum in the deep reservoirs, which dominates the phase evolution. Deep petroleum fluid phase changes mainly require the molar ratio of the input gas more than 50%. A model was proposed to explain the formation of deep condensate reservoirs. A series of gas inputs and escape in the successive lithological traps controls an orderly phase change of deep petroleum, and the amount of deeper gas determines the range of the existence of condensate gas reservoirs. This study not only guides the exploration of deep condensate in the Dongying Depression but also offers a workflow for the research on the formation and evolution of condensate reservoirs in other global regions.

1. Introduction

Global condensate gas fields are found in the West Siberian Basin, Persian Gulf Basin, Gulf of Mexico Basin, and Tarim Basin (Novikov, 2022; Milkov, 2010; Kamali et al., 2022; Thompson et al., 1990; Zhang et al., 2015). Condensate gas reservoirs produce both natural gas and condensate. These oils show significant economic value due to their low density and viscosity. Changes in temperature and pressure conditions in the reservoirs can induce the condensation of liquid from vapor, which is called retrograde condensation (Harrison et al., 2022; Igwe et al., 2022). This characteristic will bring challenges to production due to liquid condensate blocking flow channels (Haji-Savameri et al., 2020; Shi et al., 2022). Therefore, the reconstruction of the phase evolution of deep oil and gas is important as it can guide for predicting the distribution of condensates, facilitating the formulation of development strategies.

The phase behavior in petroleum fluids is tied to hydrocarbon composition, temperature, and pressure. Moreover, the hydrocarbon composition directly determines the phase envelope and critical point. Under varying temperature and pressure conditions, petroleum with the

* Corresponding author. State Key Laboratory of Petroleum Resources and Engineering, China University of Petroleum (Beijing), Beijing, 102249, China.
E-mail address: lindachen@cup.edu.cn (D. Chen).

https://doi.org/10.1016/j.marpetgeo.2024.107210
Received 16 May 2024; Received in revised form 18 October 2024; Accepted 11 November 2024
Available online 14 November 2024

same fluid composition can appear as liquid oil phase, condensate, or gas phases (Danesh, 1998; Di Primio and Horsfield, 2006). Variations in composition, temperature, and pressure may occur during hydrocarbon generation, migration, and accumulation (Hunt, 1990; Ungerer et al., 1990; Abrams, 2005). For the oil and gas accumulated in traps, fluctuations in composition, temperature, and pressure driven by geological processes control the phase states. These geological processes can be classified into two categories: (1) effects on oil and gas composition, including water washing (Lafargue and Barker, 1988; Xiong et al., 2019), biodegradation (Peters et al., 2005; Atlas and Hazen, 2011), crude oil cracking (Claypool and Mancini, 1989; Horsfield, 1992), evaporative fractionation (Thompson, 1988; Zhu et al., 2014), and TSR (Krouse et al., 1988; Zhang et al., 2019); (2) temperature and pressure reduction caused by uplift. In the case where the hydrocarbon composition remains unchanged, as temperature and pressure decrease, oil or gas can transition from single phase to gas-liquid two-phase. The formation of condensate gas reservoirs requires traps to contain enough gaseous hydrocarbons in appropriate temperature and pressure environments, providing conditions for liquids to dissolve in gases (Danesh, 1998). The main origins of gas condensate are (1) thermogenic condensate from the thermal degradation of kerogen or thermal cracking of oil (Zhang et al., 2015); (2) retrograde condensate from evaporative fractionation (Thompson, 2010); (3) paleo-oil pool mixed with late charged gases (Su et al., 2020). Additionally, the hydrocarbon phase behavior is commonly controlled by various factors under a complex geological context, adding to the challenges in reconstructing phase evolution.

Chen et al. (2019) discussed the in-situ fluid evolution in the deep light oil reservoir in the central Tarim Basin through PVT simulation and basin modeling. However, the influence of secondary alterations (e.g. crude oil cracking, water washing and TSR reaction) on hydrocarbon fluid composition was not considered. Di Primio and Horsfield (2006) used the PhaseKinetics approach to determine the compositional evolution of fluids generated in source rocks and predicted the phase behavior in time and space using petroleum system models. Fu et al. (2019) combined thermal simulation experiments and PVT simulation to construct phase diagrams of products at different evolutionary stages to approximate the fluid phase behavior in the neighboring reservoirs. Qiao and Chen (2022) revealed the phase changes during oil cracking under high temperature and pressure conditions through thermal simulation experiments. Kuske et al. (2019) predicted the fluid physical properties and composition of oil and gas in the Eagle Ford Shale using the PhaseKinetics model calibrated by a regional PVT database. Although many studies have revealed the phase evolution using various methods, some have focused on the phase behaviors of hydrocarbons within source rocks or only analyzed the phase states of in-situ oil and gas over time, lacking comprehensive simulations of petroleum phase evolution under the influence of multiple geological processes.

In recent years, breakthroughs have been made in deep oil and gas exploration in the Dongying Depression. Well FS1 encountered a condensate gas reservoir in the nearshore subaqueous fan at 4400m in the fourth member of the Shahejie Formation, achieving high oil and gas production. With the deployment of multiple exploration wells, various oil and gas phase states have been discovered in the deep strata, covering dry gas, condensate, and liquid oil. Drilling results indicate the vertical and lateral distribution ranges of various types of petroleum are challenging to determine. A lack of understanding of the formation and evolution of the reservoirs hinders effective prediction of condensate distribution, which impacts drilling strategies, development plans, and geological reserve assessments. Therefore, this study aims to reconstruct the fluid phase evolution of deep condensate gas reservoirs using a combination of fluid inclusions, PVT simulation, and basin modeling. This work achieved the following aims: (1) to restore the composition, temperature, pressure information, and phase states at each evolutionary stage; (2) to check the effect of different geological processes on petroleum phase behavior, including hydrocarbon generation, oil cracking, and gas invasion; (3) to reveal the mechanisms of formation and distribution of deep condensate gas; (4) to provide a solution for addressing the deep condensate gas evolution issues in other regions globally.

2. Geological setting

2.1. Tectonics and sedimentology

Dongying Depression is regarded as one of the important petroliferous depressions in the Bohai Bay basin (Fig. 1a and b) (Wang et al., 2019; Lei et al., 2024). The Dongying Depression is a faulted continental basin and is divided into 4 sags by faults, namely Minfeng Sag, Lijing Sag, Liuzhuang Sag, and Boxing Sag (Fig. 1b) (Hao et al., 2023). The study area is situated in the Minfeng Sag, characterized by a steep slope. The Dongying Depression underwent five stages of tectonic evolution (Song et al., 2021). (1) The early stage of fault depression (65–45 Ma). (2) The expansion stage of fault depression (45–35 Ma). (3) The stage of weakened fault activity (35–24.4 Ma). (4) The uplift and erosion stage (24.4–18 Ma). The uplift and denudation thickness averaged about 300m. (5) The late subsidence stage (18–0 Ma). Active normal faults caused the continuous subsidence.

The Paleogene Kongdian (Ek), Paleogene Shahejie (Es), Paleogene Dongying (Ed), Neogene Guantao (Ng), Neogene Minghuazhen (Nm), and Quaternary Pingyuan (Qp) formations have been filled from the early Paleozoic to the present (Fig. 1d) (Song et al., 2019). The Shahejie Formation consists of 4 members, namely, the first member of the Shahejie Formation (Es_1), the second member of the Shahejie Formation (Es_2), the third member of the Shahejie Formation (Es_3), the fourth member of the Shahejie Formation (Es_4). The Es_3 can be divided into the upper, middle, and lower parts. The Es_4 is divided into the upper and lower parts based on lithology (Fig. 1d) (Wang et al., 2022). The Es_4 is the target layer of this study, which is a typical continental saline environment, with lithology covering gray-black mudstone, sandstone, and conglomerate, and interbedded with grayish-white gypsum-salt rock and gray mudstone (Fig. 1d) (Liu, 2022). The sand body extends from the steep slope zone to the sag and covers a large area formed in a rapid depositional context (Fig. 1c).

2.2. Petroleum system

In this study, the fourth member of the Shahejie Formation (Es_4) is the investigative interval, which is buried at a depth exceeding 3500m. The Dongying Depression was a huge saline lake during the sedimentary period of the Es_4 (Jia et al., 2013). Therefore, the gray-black shale and gypseous mudstone are the main high-quality source rocks consisting of type I-II organic matter. More than 80% of the source rocks bear a total organic carbon (TOC) content greater than 2% with a high mature or over-mature stage (Liu, 2022). The nearshore subaqueous fan deposited in the steep slope zone provides traps and reservoirs for deep hydrocarbons. However, the porosity of pebbly sandstones in the middle fan ranges from 1.4% to 10.7%, and their permeability is between 0.02–27.6 mD, showing a strong heterogeneity in physical properties. The porous pebbly sandstones have average values of porosity and permeability of 6.8% and 1.42 mD, respectively, serving as the main reservoir (Song et al., 2019). The sandstones or mudstone interlayers with low permeability act as cap rocks to block the upward migration (Fig. 2). The proximal fan is dominated by muddy conglomerates with an average permeability of 0.21 mD, which prevents lateral hydrocarbon migration. As a result, the deep oil and gas are generated from the adjacent mature source rocks and migrated laterally into the middle fan sandstones (Yang et al., 2023). These seals are made of low permeability rocks formed around the reservoir, blocking the oil and gas inside the lithologic traps (Fig. 2). A variety of petroleum phases is developed vertically, including dry gas, condensate, and light oil (Fig. 2) (Wang et al., 2023). The wells FS1, FS1-X1, and FSX101 encountered deep condensate gas reservoirs

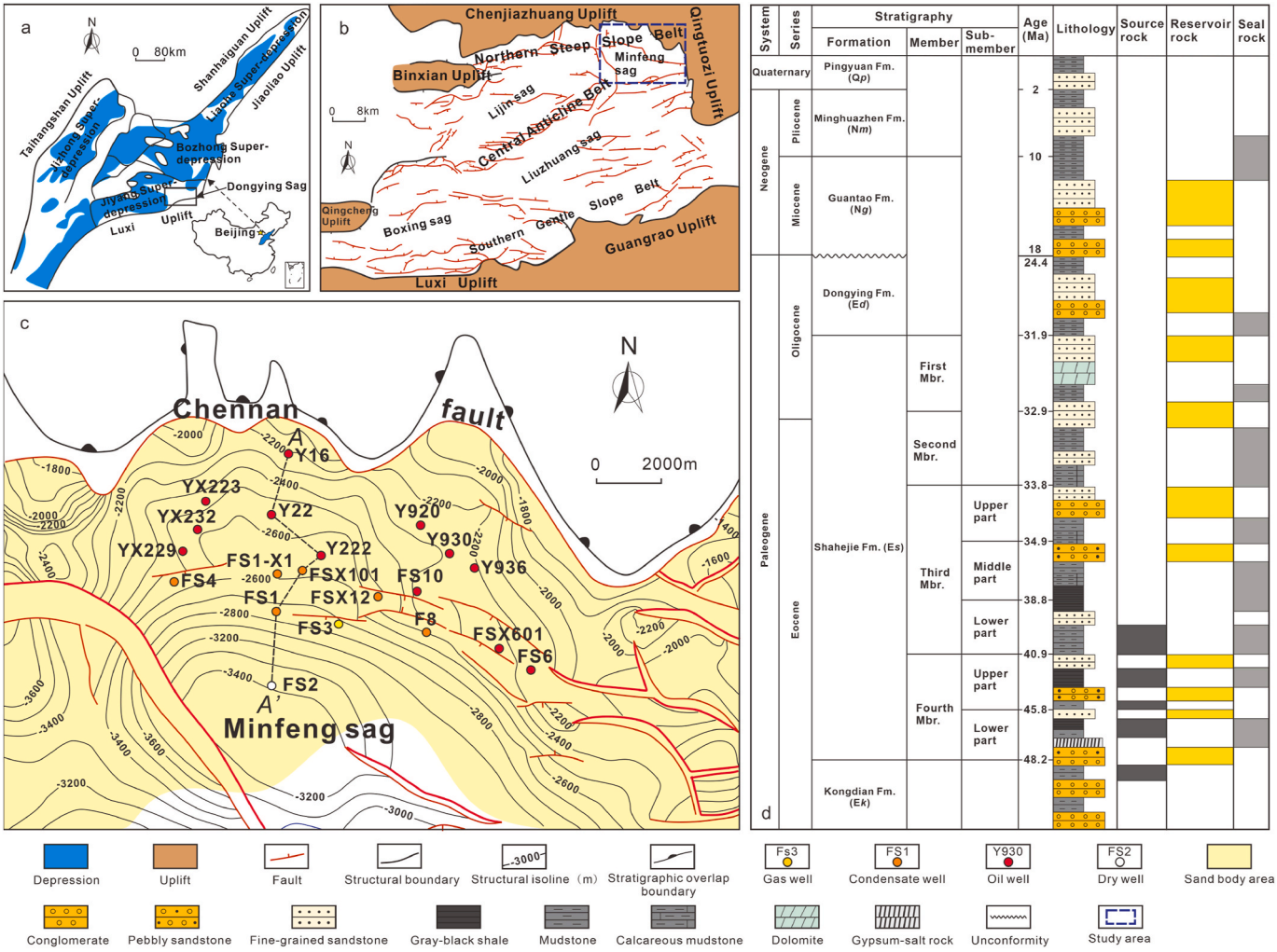

Fig. 1. (a) Location and simple structural pattern map of the Bohai Bay Basin. The Dongying Depression is located at the east of the Jiyang Super-depression, Bohai Bay basin. (b) Structural unit map of the top surface of the fourth member of the Shahejie Formation in the Dongying Depression. The study area is located in the northeast of the Dongying Depression and is marked by a dotted line. (c) Structural map and sand body distribution of the study area. The circles with colors indicate different production wells of deep petroleum, including gas, oil, and condensate. (d) Stratigraphic column and petroleum system elements of the Dongying Depression. The data of stratigraphical age refers to Yao et al. (2007).

with a burial depth greater than 4300m (Fig. 2).

3. Methods and data

3.1. Sampling and data

This study collected 4 and 3 core samples from the condensate gas reservoirs of wells FS1 and FSX101, respectively. These samples were supported by Sinopec Shengli Oilfield (Fig. 2). Meanwhile, the oilfield provided the condensate samples from wells FS1, FS1-X1, and FSX101 under the surface at a depth of approximately 4300m for a detailed PVT experiment to obtain hydrocarbon components (Fig. 2). The composition information of the deep condensate gas will be employed to correct the simulated fluid phase state. Furthermore, Sinopec Shengli Oilfield provided test data that includes formation temperature and formation pressure. The vitrinite reflectance R_o of the deep source rocks was analyzed in the laboratory of the Shengli Oilfield. The physical properties of condensates (density, viscosity, and GOR) were measured at the State Key Laboratory of Petroleum Resources and Engineering, China University of Petroleum (Beijing). This data will be used to calibrate the basin modeling for petroleum fluid phase reconstruction.

3.2. Fluid inclusion analysis

The core samples were finely ground into thin sections approximately 100 μm in thickness and utilized for volumetric and microthermometric measurements conducted at the China National Nuclear Corporation (CNNC) Analytical Laboratory of the Beijing Research Institute of Uranium Geology (BRIUG). The prepared thin sections were observed using a standard Nikon 80I microscope equipped with an ultraviolet light source. First, the host mineral of each inclusion was identified under transmitted light mode, followed by a switch to ultraviolet light mode to identify hydrocarbon inclusions. The occurrence and fluorescence color were recorded systematically. Furthermore, the diagenetic condition and period when the fluid was trapped can be determined based on the occurrence of inclusions. The fluorescent color of oil inclusions can indicate maturity (Hagemann and Hollerbach, 1986; Stasiuk and Snowdon, 1997). As maturity increases, the fluorescent colors take on a yellow, blue-green, blue-white, blue, and nonfluorescent successively (Ping et al., 2017). In addition, the fluorescence color can indirectly reflect the fluid phase condition, as high-maturity petroleum usually has a high percentage of gas-phase components.

Homogenization temperatures (Th) of fluid inclusions were determined by a LINKAM (THMS600) cooling-heating stage, and the measurement precision was within ±0.1 °C. The confocal laser scanning

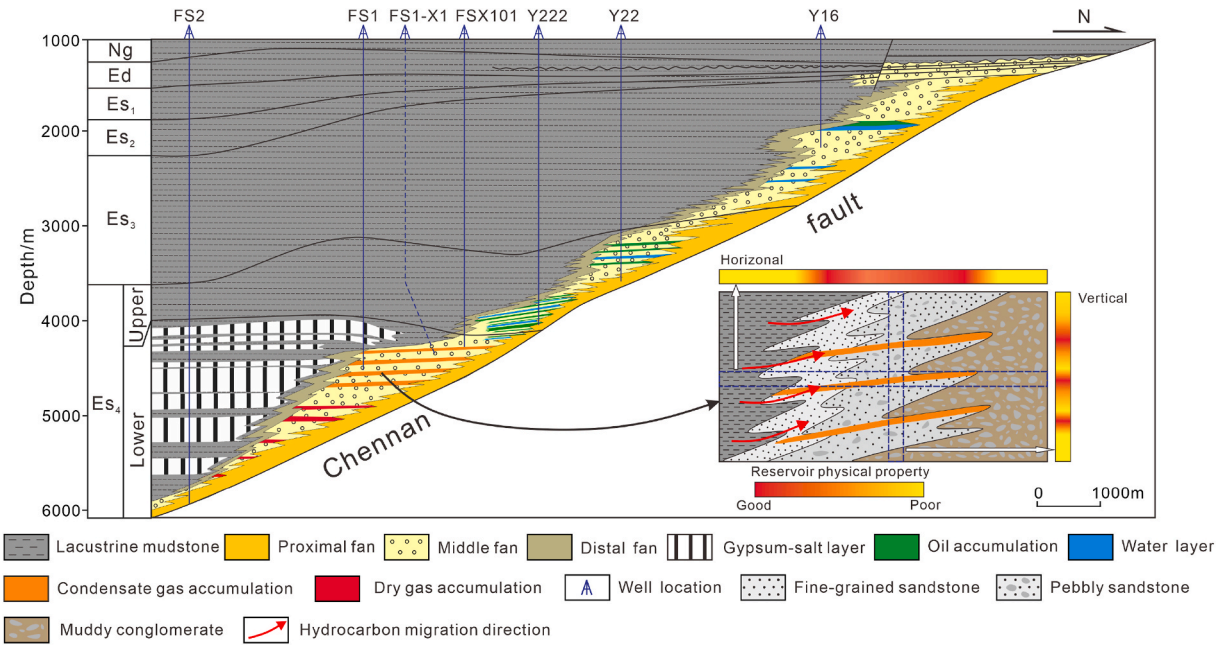

Fig. 2. Petroleum system of deep hydrocarbons in the Dongying Depression. Oil and gas are accumulated in the pebbly sandstones of the middle fan and generated from the lateral lacustrine mudstones. Lithologic traps are widely developed due to the heterogeneity in reservoir physical properties. Well FS1-X1 was projected onto this profile.

microscope (CLSM) was used to measure the volume of vapor phase to liquid phase within an individual oil inclusion at 20 °C to calculate the vapor filling degree (F_v) (Pironon et al., 1998; Aplin et al., 1990). The composition of an individual petroleum inclusion was modeled using the method proposed by Aplin et al. (1990). Based on the volumetric ratio of vapor and liquid of included petroleum (F_v) and its homogenization temperature (Th_{oil}), an iteration of PVT properties can be used to calculate its composition, phase envelope, and isochore. The series of processes can be implemented in PVT simulation software. The procedure and details of the calculation are referred to Aplin et al. (1990). Furthermore, the Th of coeval aqueous inclusion can be combined with the thermal burial history to determine the trapping time and depth of the inclusion. Therefore, based on the paleo reservoir temperature and pressure, the composition and phase envelope of the petroleum captured in different oil and gas charging periods can be obtained.

3.3. 2D basin modeling

3.3.1. Basin model construction

In this study, two-dimensional (2-D) basin modeling was performed to reconstruct the generation, migration, accumulation, and phase evolution of the deep condensate gas using the 2D module of PetroMod 2016.1 software developed by Schlumberger. The south-north cross-section of a single fan body in the northern Dongying Depression was selected to minimize hydrocarbon lateral migration and leakage (Fig. 2). This profile covers several types of petroleum reservoirs, especially deep condensate, and includes other petroleum system elements.

A series of customized mixing lithology was constructed for the 2D model and the details of mixing are shown in Table 1. Next, the facies definition was carried out, which is essential for a realistic simulation. The term “facies” contains lithology, source rock geochemical parameters, and hydrocarbon generation kinetics. It is used to assign geological properties to different locations in the simulated profile. The gold tube thermal simulation of the low mature Es_4 source rock (type I kerogen) in the Dongying Depression was conducted by Sun et al. (2019) to obtain the kinetic parameters. The average activation energy of the Es_4 source rock is 53 kcal/mol with a frequency factor A of 5.00E+15 s^{-1}, which is similar to the boghead coal sample of the United States from lacustrine depositional environments. Meanwhile, the burial depth of the Es_4 source rock is over 3500m with the maturity ranging from mature to over-mature. Hydrocarbon secondary cracking at high maturity stages should be considered. Therefore, the T1_Boghead_coal compositional kinetics model combined with a secondary cracking model was selected to simulate the petroleum composition during generation and thermal cracking (Fig. 3) (Di Primio and Horsfield, 2006; Kauerauf and Hantschel, 2009). The TOC and HI data of the Es_4 source rock were derived from the Shengling Oilfield. Based on the deep hydrocarbon accumulation simulation, nine types of facies were defined and are listed in Table 2. The naming of facies used lithology plus sedimentary environment. Furthermore, the sedimentary strata were divided into several sublayers to enhance the simulation resolution, showing the vertical variation in the same formation. Based on the well-logging and core data, the two-dimensional geological model was constructed through facies assignment (Fig. 4). Meanwhile, the trap-filling model has been characterized according to the understanding of the petroleum system and the sedimentary facies. The porous sandstones within the middle fan are sealed by low-permeability proximal fan muddy conglomerate, mudstone, and gypsum-salt rocks, forming lithologic traps (Song et al., 2019). The oil and gas in the trap can escape from the spill point and migrate upward (Fig. 4b). These stacked traps develop at the edges of the depression. The location marked by a yellow star indicates the condensate gas reservoirs for phase evolution reconstruction in this study.

Table 1
The customized lithology for 2D basin modeling of the Dongying depression.

Customized lithology	Lithology and ratio for mixing
Argillaceous sandstone	70% sandstone (typical) + 30% shale (organic lean, typical)
Pebbly sandstone	75% sandstone (typical) + 25% conglomerate (typical)
Sandy mudstone	30% sandstone (typical) + 70% shale (typical)
Muddy conglomerate	60% conglomerate (typical) + 40% shale (organic lean, typical)
Gypseous mudstone	70% shale (organic-rich, 3% TOC) + 30% gypsum
Argillaceous gypsum	65% gypsum + 30% shale (typical)
Gypsolyte-salt rock	55% gypsum + 45% salt

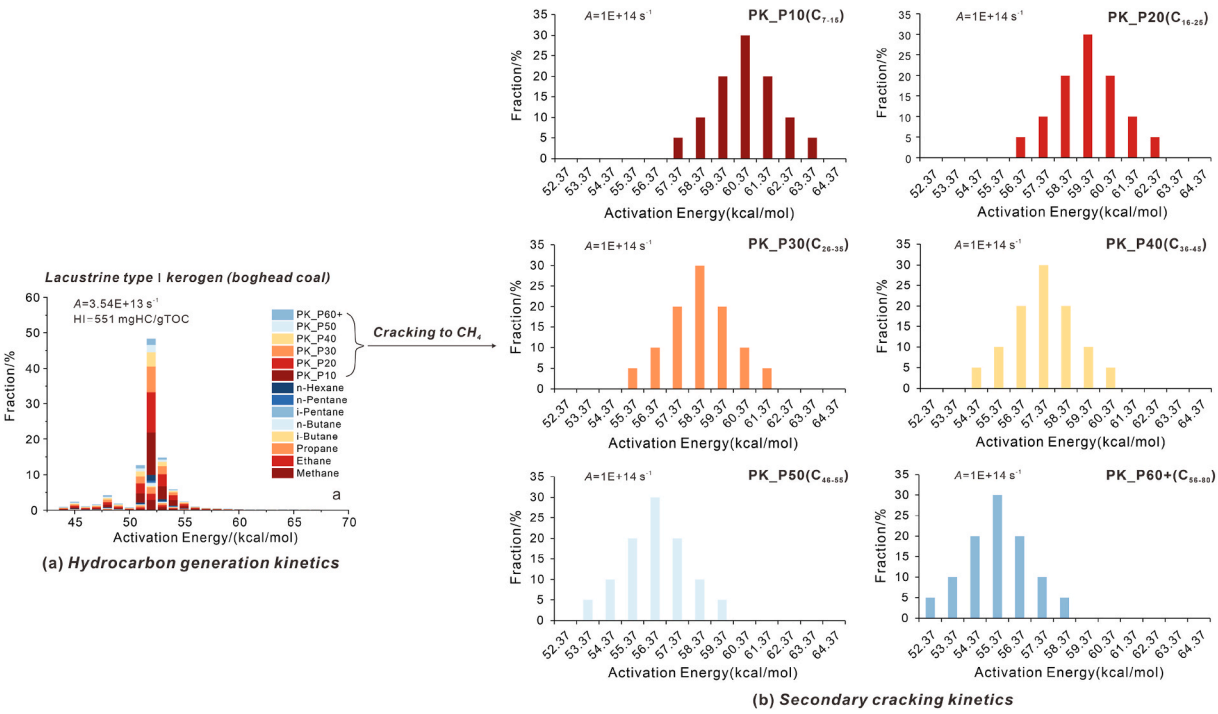

Fig. 3. (a) The primary cracking kinetic model of the lacustrine boghead coal from the United States (Di Primio and Horsfield, 2006); (b) Secondary cracking kinetic parameters of the heavy hydrocarbon components (Kauerauf and Hantschel, 2009).

Table 2
The defined facies showing different lithology and geochemical parameters. The T1_Boghead_Coal_Crack kinetic model was chosen for primary hydrocarbon generation simulation. The term source rock is abbreviated as SR.

Facies name	Lithology	Kinetics	TOC (%)	HI (mgHC/gTOC)	Petroleum system elements
Quaternary mudstone_facies	Shale (organic lean, silty)				Seal rock
Fluvial and deltaic argillaceous sandstone_facies	Argillaceous sandstone				Reservoir rock
Freshwater deep lacustrine mudstone_facies	Shale (organic-rich, 3% TOC)	T1_Boghead_Coal_Crack	5.5	544	Source rock
Saline lacustrine mudstone_facies	Gypseous mudstone	T1_Boghead_Coal_Crack	5	495	Source rock
Freshwater shallow lacustrine mudstone_facies	Sandy mudstone	T1_Boghead_Coal_Crack	3.5	443	Source rock
Saline lacustrine evaporite_facies	Gypsolyte-salt rock				Seal rock
Saline lacustrine argillaceous evaporite_facies	Argillaceous gypsum				Seal rock
Middle fan and distal fan sandstone_facies	Pebbly sandstone				Reservoir rock
Proximal fan conglomerate_facies	Muddy conglomerate				Seal rock
Gneiss basement_facies	Gneiss				Underburden rock

3.3.2. *Parameters for modeling*

The stratigraphic ages were derived from Yao et al. (2007). The paleo-water depth data of the Dongying Sag utilized in the simulation were obtained from Bo (2008). The sedimentary water interface temperature (SWIT) values can be calculated from the sea level temperature after a transformation that corrects the surface temperature against the paleo water depth (Peters et al., 2017). In this study, the Dongying Depression is located in the Northern Hemisphere at a latitude of 35° in Eastern Asia and the SWIT values were obtained by automatic transformation in the PetroMod software. The EASY% R_o model was utilized to calculate the vitrinite reflectance (R_o) (Sweeney and Burnham, 1990). The heat flow values were referred from Bo (2008) and the thermal parameters were adjusted to match the present-day formation temperature and R_o data. The migration method used in the 2D basin modeling is the combined approach, which uses Darcy flow in low permeability units and invasion percolation in high permeability units such as carriers and reservoir beds (Hantschel and Kauerauf, 2009; Baur et al., 2011).

3.4. *Fluid phase simulation*

PVTsim 20 software developed by Calsep was used to calculate the phase envelope, critical temperature, and critical pressure. The Soave-Redlich-Kwong equation of state (SRK-EoS) was selected in the PVT simulation (Soave, 1972). Based on the composition (Mol%), molar mass, and liquid density of hydrocarbon components, the fluid database was constructed and different heavy reservoir fluids were characterized to a unique set of pseudo-components, which is advantageous for compositional simulation. Here, the components of reservoired condensate were obtained from the PVT experiment in the laboratory, and the numerical simulation results in the software should be consistent with the experimental data. Furthermore, the phase states of oil inclusions were reconstructed based on the composition, paleo-temperature, and paleo-pressure. The temperature and pressure evolution can be obtained from the basin modeling results.

Due to the introduction of the compositional kinetic and secondary cracking model into basin modeling, the simulated fluid composition was described as 14 components, including methane (CH_4), ethane (C_2H_6), propane (C_3H_8), i-butane (i-C_4H_{10}), n-butane (n-C_4H_{10}), i-pentane (i-C_5H_{12}), n-pentane (n-C_5H_{12}), n-hexane (n-C_6H_{14}), and 6 pseudo-components (Fig. 3). The six pseudo-component PK_P10, PK_P20, PK_P30, PK_P40, PK_P50, and PK_P60+ grouped $C_{7\text{-}15}$, $C_{16\text{-}25}$, $C_{26\text{-}35}$, $C_{36\text{-}45}$, $C_{46\text{-}55}$, and $C_{56\text{-}80}$ carbon number ranges, respectively. The fluid phase variation of the deep reservoir during hydrocarbon generation-migration-accumulation was simulated by defining the

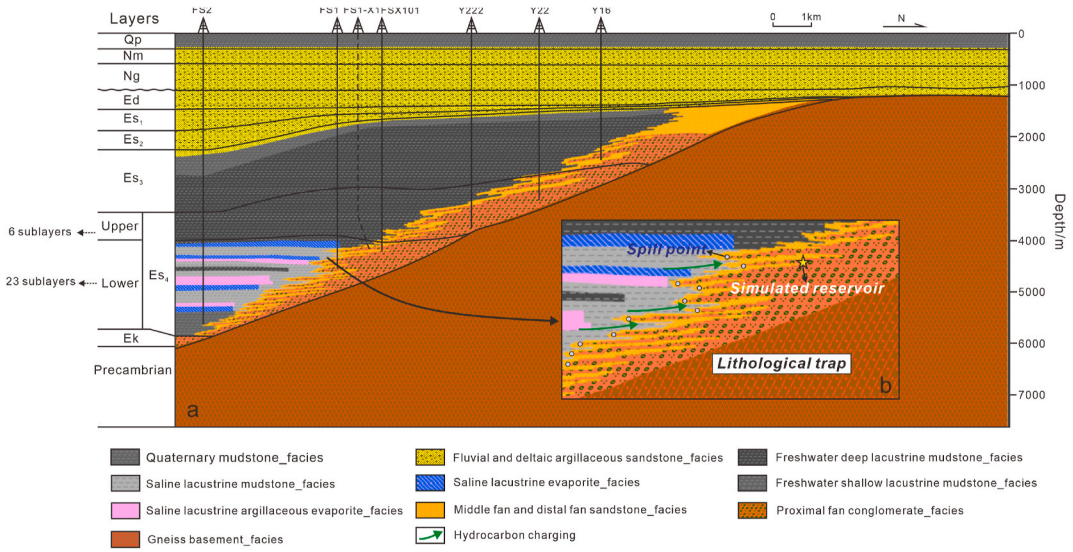

Fig. 4. (a) The constructed 2D geological model showing the strata and facies. The stratigraphic framework is based on the seismic interpretation from the oilfield. Well FS1-X1 is projected on the profile. The profile location is shown in Fig. 1. (b) The trap-filling model is developed based on the petroleum system and sedimentary facies of the northern Dongying Depression, showing the petroleum accumulation and spilling. The burial depth of the simulated reservoir is consistent with the present condensate pools (~4320 m).

pseudo-components.

3.5. Workflow of fluid phase evolution reconstruction

The primary approach to reconstructing the fluid evolution of deep condensate gas reservoirs involves utilizing the compositions of oil inclusions and the high-pressure physical properties of current condensates as the point information on the evolutional sequence to constrain the basin model, thereby obtaining a reliable complete fluid phase evolution process (Fig. 5). The detailed processes are as follows.

(1) Identify oil inclusions and coexisting aqueous inclusions in deep condensate gas reservoirs. The F_v and Th_{oil} of an individual petroleum inclusion are brought into the petroleum inclusion thermodynamic model to calculate the hydrocarbon composition, while the PVT simulation software is applied to calculate the phase diagram and critical point.
(2) The forming period and fluid phase types of the hydrocarbon inclusions are identified based on the occurrence and fluorescent color. The trapping time of oil inclusion is determined by combing the Th_{aqu} and burial and thermal histories derived from basin modeling. The petroleum phase state in the reservoir during the trapping period is identified through the phase envelope of the included oil and the paleo-temperature and pressure.
(3) Establish a basin model with appropriate compositional kinetics and secondary cracking kinetics to simulate the reservoired hydrocarbon components during hydrocarbon generation, migration, and accumulation. The condensate compositional data, density (20 °C, 0.101 MPa), viscosity (20 °C, 0.101 MPa), and gas-oil ratio (GOR) are used to calibrate the modeled present-day oil and gas. The simulated compositions of different geological periods are constrained by the component information obtained from petroleum inclusions.
(4) Adjust the parameters of the basin model until the simulated values match the inclusion data and the wellstream sample data. The final reconstructed phase evolution of deep condensate gas is obtained. The detailed adjustments and measured data for calibrating the basin model are presented in Section 4.3.1.

4. Results

4.1. Fluid characteristics of present-day condensate gas reservoir

The phase envelope calculations and the petroleum samples of the 3 wells were obtained from condensate gas reservoirs with similar depths and reservoir conditions (formation temperature and pressure). Furthermore, the density of these fluids ranges from 0.77 g/cm^3 to 0.78 g/cm^3 at standard temperature and pressure. The wellstream sample from well FSX101 has a relatively high viscosity of 1.62 mPa s compared to the other two wells. The fluid samples have the measured gas-oil ratios over 2000 m^3/m^3, among which well FS1 has the highest value, reaching 2857 m^3/m^3 (Table 3). Thus, drilling in the deep reservoirs often produces both oil and natural gas with a high proportion of natural gas.

The hydrocarbon compositions and PVT properties of these 3 petroleum samples are shown in Table 4 and Table 5, respectively. The critical point was not calculated for the sample from well FSX101, probably because the condensate contains few heavy components and the critical temperature is low. The heavy components would convert to solids at low temperatures, making it impossible to calculate the critical point. Meanwhile, the cricondenbar and cricondentherm of hydrocarbon fluids in well FSX101 are higher than those in FS1 and FS1-X1 (Table 4). The petroleum composition indicates that the deep petroleum in the three wells is all condensate gas (Fig. 6a). These fluid samples are considered to maintain a condensate gas phase under reservoir conditions (Fig. 6b, c, d).

4.2. Fluid phase reconstruction of petroleum inclusions

4.2.1. Fluid inclusion petrography and microthermometry

In the deep condensate gas reservoirs of the Dongying Depression, a large number of fluid inclusions are developed. A total of 61 inclusions were identified and measured under the microscope in this study. Feldspar is the main host mineral for petroleum inclusions (Fig. 7). The reservoir mostly contains gas-liquid phase hydrocarbon inclusions, with hydrocarbons mainly filling the dissolution pores of feldspars (Fig. 7c_1, d_1, f_1, g_1, h_1). A small portion of hydrocarbons are trapped in secondary microfractures of quartz and calcite cement (Fig. 7a_1, b_1, e_1). Numerous coeval brine inclusions with similar occurrences surround the

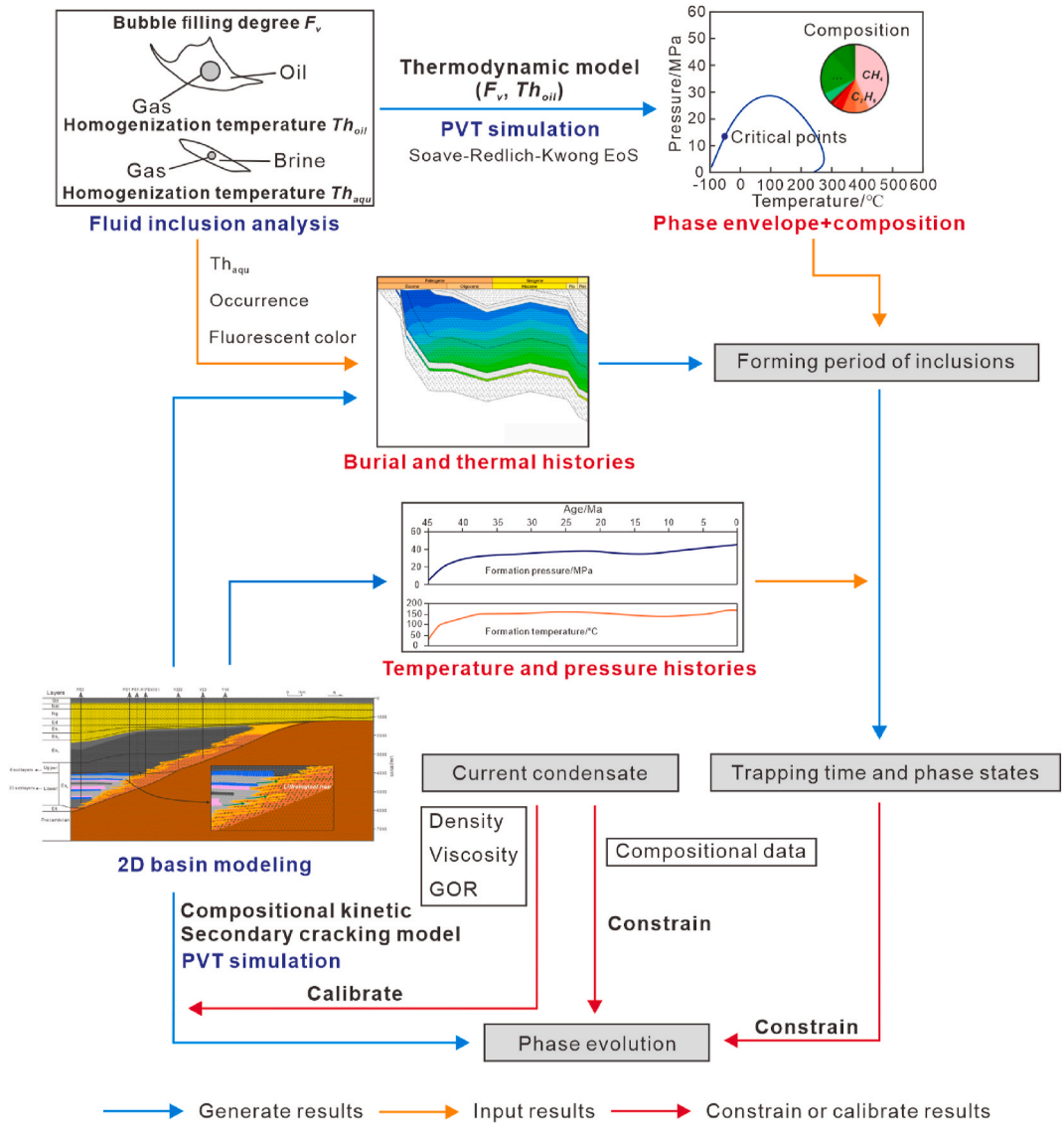

Fig. 5. The basic workflow for phase evolution reconstruction.

Table 3
The physical properties of condensate gas samples from wells FS1, FS1-X1, and FSX101 in a standard condition (20 °C, 0.101 MPa).

Well name	Depth of the middle part of reservoirs (m)	Reservoir temperature (°C)	Reservoir pressure (MPa)	Density (g/cm^3)	Viscosity (mPa·s)	GOR (m^3/m^3)
FS1	4330	185	43.9	0.78	0.72	2857
FS1-X1	4285	171	42.7	0.77	0.81	2048
FSX101	4241	165	42.2	0.78	1.62	2250

Table 4
The PVT properties of condensate gas samples from wells FS1, FS1-X1, and FSX101 derived from the PVT experiment.

Well name	Depth of the middle part of reservoirs (m)	Dew point pressure at formation temperature (MPa)	Critical pressure (MPa)	Critical temperature (°C)	Cricondenbar (MPa)	Cricondentherm (°C)
FS1	4330	35.10	34.02	58.16	36.86	358.1
FS1-X1	4285	22.29	22.43	41.15	24.19	273.84
FSX101	4241	41.66	\	\	42.97	370.9

hydrocarbon inclusions (Fig. 7). Additionally, under fluorescence mode, hydrocarbon inclusions with yellow, blue-green, blue-white, and blue fluorescence were observed (Fig. 7). The fluid inclusions were classified based on their fluorescence colors, and microthermometry was conducted on the petroleum inclusions and coeval aqueous inclusions. The results show that the temperatures of the yellow fluorescent oil inclusions homogenized to a vapor phase ranged from 120 °C to 135 °C. The homogenization of the vapor bubbles into a single phase in their coeval aqueous fluid inclusions occurred between 140 °C and 160 °C (Fig. 8a). The homogenization temperatures of the blue-green

Table 5
The compositional data of the wellstream from the condensate gas reservoirs of wells FS1, FS1-X1, and FSX101.

Well name	Depth of the middle part of reservoirs (m)	Component (Mol, %)														
		N_2	CO_2	C_1	C_2	C_3	iC_4	nC_4	iC_5	nC_5	C_6	C_7	C_8	C_9	C_{10}	C_{11+}
FS1	4330	0.35	6.80	81.76	3.44	1.70	0.33	0.66	0.54	0.51	1.80	0.99	0.21	0.14	0.12	0.68
FS1-X1	4285	3.23	0.75	71.15	5.73	4.57	1.67	3.17	1.86	1.56	3.11	1.44	0.32	0.24	0.21	0.98
FSX101	4241	/	3.43	81.40	8.99	1.71	0.25	0.50	0.14	0.16	0.28	0.22	0.37	0.51	0.38	1.67

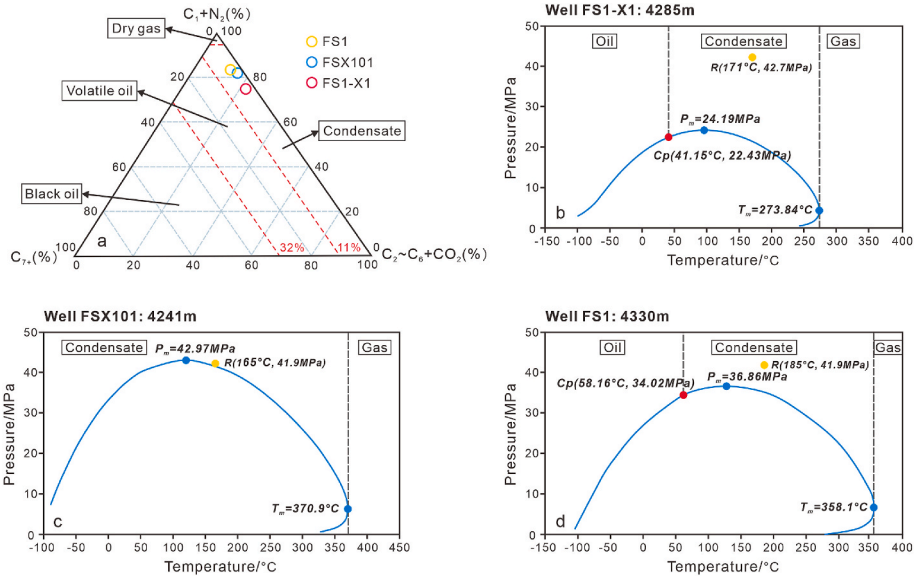

Fig. 6. (a) A triangle method for fluid phase discrimination by petroleum compositions. (b–d) The phase envelopes of the petroleum samples from wells FS1-X1, FSX101, and FS1, showing the critical temperature and pressure. Based on the phase diagrams, these fluids remained in condensate phase states under the reservoir conditions.

fluorescent oil inclusions and coeval brine inclusions range from 125 °C to 140 °C and from 145 °C to 165 °C, respectively (Fig. 8b). The aqueous fluid inclusions coexisting with the blue-white fluorescent inclusions homogenized to mono-phase liquid at the temperatures between 145 °C and 165 °C. Furthermore, the homogenization temperatures of these petroleum inclusions ranged from 135 °C to 150 °C (Fig. 8c). The vapor bubbles disappeared in the blue fluorescent inclusions at temperatures between 150 and 160 °C, and the coeval brine inclusions homogenized to a single phase at temperatures ranging from 175 to 185 °C (Fig. 8d).

A total of 8 petroleum inclusions with various fluorescence colors were selected for the determination of the gas-liquid volume ratio at room temperature. The microthermometry results and the degrees of gas bubble filling (F_v) are shown in Table 6. Yellow fluorescence was observed in inclusion 1, with a gas phase volume fraction of 16.17% (Fig. 7a_1, a_2). Inclusion 2 and 3 exhibit blue-green fluorescence, with gas filling degrees of 19.77% and 22.94%, respectively (Fig. 7b_1, b_2, c_1, c_2). Inclusions 4 and 5 show blue-white fluorescence with gas-liquid volume ratios of 31.58% and 27.23%, respectively (Fig. 7d_1, d_2, e_1, e_2). The bubbles in blue fluorescent oil inclusions can occupy up to 50% of the volume, represented by inclusions 6 and 7 (Fig. 7f_1, f_2, g_1, g_2). The bubble volume ratio of inclusion 8 was 44.86% (Fig. 7h_1, h_2). In the study conducted by Ping et al. (2012), a sample with the F_v reaching 72.5% was measured in the condensate gas reservoir of well FS1 and designated as inclusion 9.

4.2.2. *Hydrocarbon compositions and trapping time of petroleum inclusions*

Hydrocarbon fluid inclusions serve as a valuable source of paleo-fluid information, enabling the determination of paleo-temperature, paleo-pressure, and fluid composition. The composition information of the above 9 hydrocarbon inclusions was reconstructed based on the petroleum inclusion thermodynamics. From yellow inclusion 1 to blue inclusion 9, the methane content increases from ~40% to ~80%, while the proportion of heavy hydrocarbons (C_{11+}) decreases gradually from ~20% to ~5% (Fig. 9a, Table 7). The fluorescence color of oil inclusions is correlated with hydrocarbon composition, shifting from yellow to blue-green, blue-white, and blue as heavy components decrease and light components increase. This phenomenon is in line with the findings of Goldstein and Reynolds (1994).

Temperature, pressure, and composition are key parameters determining the phase behavior of oil and gas. Basin modeling was utilized to reconstruct the ancient pressures and temperatures at the time of fluid inclusion formation (Fig. 9c and d). The information regarding the calibration of basin modeling can be found in Section 4.3.1. Generally, the homogenization temperature of brine inclusions coexisting with petroleum inclusions, combined with burial and thermal histories, can determine the trapping time for oil inclusions, although this result may be ambiguous (Guo et al., 2012; Volk and George, 2019) Therefore, the trapping time needs to be constrained by reservoir diagenesis and fluid inclusion petrography to eliminate interpretational ambiguity (Goldstein, 2001). Yellow oil inclusions formed between ~39.8 Ma and ~38.7 Ma, corresponding to the early period of the first phase of hydrocarbon generation. Blue-green oils were trapped from ~36.7 Ma to 24.7 Ma. The trapping time of blue-white fluorescent inclusions ranged from ~24 Ma to ~18 Ma, coinciding with the late period of the first phase of hydrocarbon generation, during the uplift and erosion event of the Dongying Depression, facilitating hydrocarbon release and migration (Guo et al., 2020). The blue fluorescent oil inclusions were trapped during the period of 5–0 Ma (Table 6, Fig. 9c).

Trapped petroleum fluid phases can be identified by combining phase diagrams with temperature-pressure data. The phase diagrams reconstructed using PVT simulation software based on the component data show that the petroleum in yellow fluorescent inclusion 1 displays a

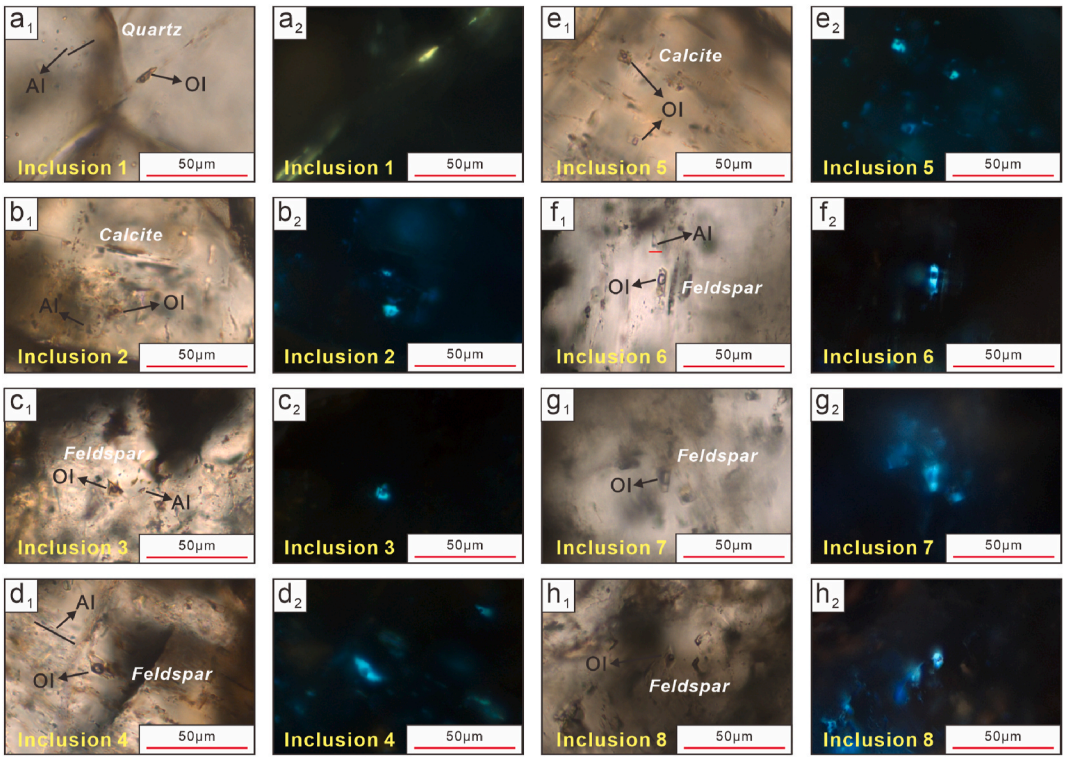

Fig. 7. Photomicrographs showing occurrence and fluorescent color of the representative petroleum fluid inclusions and brine inclusions in plane-polarized light (PPL; a_1, b_1, c_1, d_1, e_1, f_1, g_1, h_1) and ultraviolet light (UV; a_2, b_2, c_2, d_2, e_2, f_2, g_2, h_2) from the deep condensate gas reservoirs in the Dongying Depression. In this figure, x_1 and x_2 are in the same field of view (x = a, b, c, d, e, f, g, h). (1) a_1 and a_2 show a two-phase yellow fluorescent petroleum inclusion in a healed microfracture of quartz in the well FS1. (2) b_1 and b_2 show a petroleum inclusion hosted in calcite cement that has blue-green fluorescence under UV in the well FS1. (3) c_1 and c_2 show a blue-green fluorescent petroleum inclusion in a healed dissolution pore of feldspar in the well FS1. (4) d_1 and d_2 show a petroleum inclusion in a healed dissolution pore of feldspar, with a gas bubble and blue-white fluorescing oil in the well FS1. (5) e_1 and e_2 show a two-phase blue-white petroleum inclusion hosted in calcite cement in the well FS1. (6) f_1 and f_2, g_1 and g_2, and h_1 and h_2 all show two-phase petroleum inclusions displaying intense blue fluorescence color hosted in feldspar in the well FSX101.

high critical temperature and a low critical pressure. This suggests the early heavy oil was trapped by inclusion 1 around 39Ma (Fig. 9b and c). Inclusions 2 and 3 show a decrease in critical temperature and an increase in critical temperature compared to inclusion 1, with the phase envelope line stretching upwards. The included hydrocarbon fluids were trapped in a liquid phase between ~31 Ma and ~25 Ma (Fig. 9b and c). The phase diagrams of inclusions 4 and 5 show the critical points shifting towards the upper left, indicating the trapped unsaturated light oil during the uplift and erosion period (24–20 Ma) (Fig. 9b and c). The phase diagrams of blue fluorescent inclusions 6, 7, and 8 indicate a variety of fluid phase states between ~3 Ma and 2 Ma (Fig. 9b and d). The included petroleum in inclusions 6 and 8 remained in a liquid phase with characteristics similar to volatile oil. The paleo-reservoir temperatures of inclusion 7 and 9 are significantly higher than the critical temperatures, and the pressures are above the dew point line, indicating that the trapped petroleum was in a condensate gas phase. Compared to the phase diagram of inclusion 7, inclusion 9 shows a notable reduction in critical temperature and pressure, with the critical point dropping to the lowest value region (Fig. 9b). The oil inclusions formed in the second phase of hydrocarbon generation mark a critical phase transition period in the deep oil and gas reservoirs.

4.3. 2D basin modeling

4.3.1. Calibration of the basin modeling

Thermal calibration is crucial for a 2D basin model to yield reasonable results. The vitrinite reflectance curve calculated by the EASY R_o model fits well with the measured data from well FS1 and neighboring wells, achieved by adjusting the value of heat flow and the thermal conductivity of rocks (Fig. 10a). Additionally, the simulated temperature trend closely matches the measured formation temperatures (Fig. 10a), indicating that the established basin model can effectively evaluate the thermal evolution history and the timing of hydrocarbon generation and expulsion. The petroleum physical properties are important indicators of fluid phase behavior. When the modeled physical properties are similar to the sample data, the calculated fluid compositions can be more reliable. These physical properties are highly related to hydrocarbon generation kinetics and thermal conditions. Thus, reasonable kinetics and calibrated thermal parameters are important for fluid phase modeling. The modeled density of the present-day condensate at 20 °C and 1atm is 800 kg/m^3 (0.8 g/cm^3), with a viscosity of 2.08 mPa s and a gas-oil ratio of 2137 m^3/m^3, which is similar to the physical properties of the wellstream fluids from wells FS1, FS1-X1 and FSX101 (Fig. 10b, c, d, Table 3). Additionally, the evolution curves of physical parameters show rapid increases or decreases after 5 Ma. The fluid composition directly determines the phase envelope, making phase diagrams as the parameters with high constraints on the results of 2D basin simulation. Thus, adjusting the parameters related to expulsion and migration until the simulated condensate gas phase diagram matched the phase diagrams of the condensate oil sample and petroleum inclusion 9. Key parameters include the mechanical compaction curve, the relationship between porosity and permeability, and capillary entry pressure (preferably based on experimental data). These parameters influence the efficiency of hydrocarbon expulsion and migration. Based on the trap-filling model and the simulated hydrocarbon compositions, adjustments are made to the expulsion and charging volumes to change the composition. Fig. 10e shows that the deep condensate gas phase diagram generated by the 2D model is similar

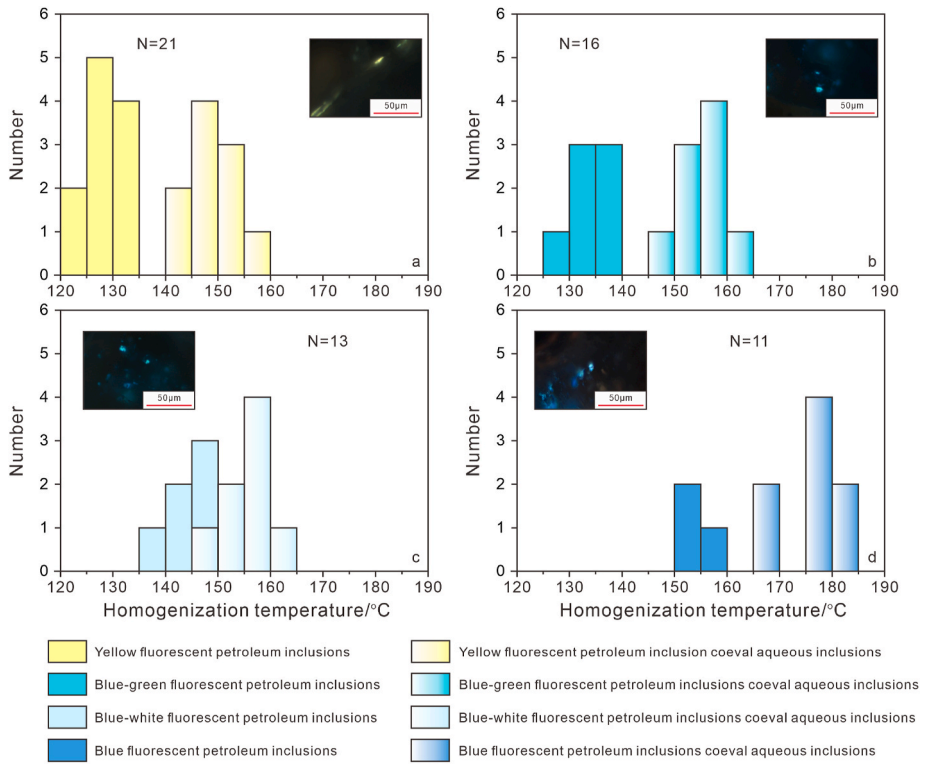

Fig. 8. Histograms of homogenization temperature of petroleum inclusions with different fluorescent colors and coeval aqueous inclusions from the deep condensate gas reservoirs in the Dongying Depression.

Table 6
Microthermometry data and petrographic features of the eight oil inclusions and coeval aqueous fluid inclusions. The gas filling degrees were measured for the petroleum inclusions.

Number	Well name	Depth (m)	Lithology	Occurrence	Fluorescence color	Th_{oil} (°C)	Th_{aqu} (°C)	F_v (%)	Trapping time (Ma)
Inclusion 1	FS1	4349.7	Pebby sandstone	Microfracture in quartz	Yellow	128	148–150	16.17	39.2
Inclusion 2	FS1	4348.5	Fine sandstone	Calcite cement	Blue-green	134	152–155	19.77	31.6
Inclusion 3	FS1	4348.5	Fine sandstone	Feldspar dissolution pore	Blue-green	131	159–160	22.94	25.2
Inclusion 4	FS1	4322.9	Pebby sandstone	Feldspar dissolution pore	Blue-white	137	151–153	31.58	20.1
Inclusion 5	FS1	4322.9	Pebby sandstone	Calcite cement	Blue-white	140	157–158	27.23	23.6
Inclusion 6	FSX101	4530.8	Conglomerate	Feldspar grain	Blue	156	177	55.39	2.8
Inclusion 7	FSX101	4528.5	Pebby sandstone	Feldspar grain	Blue	158	178	57.49	2.4
Inclusion 8	FSX101	4528.5	Pebby sandstone	Feldspar grain	Blue	156	171	44.87	2.4
Inclusion 9[a]	FS1	4321.7	Pebby sandstone	Quartz grain	Blue	150.3	178.7	72.50	2

[a] The measured results of the inclusion 9 were obtained from Ping et al. (2012).

to the phase diagrams of the oil sample and petroleum inclusion. Furthermore, the hydrocarbon component distribution of the investigated reservoir obtained through basin modeling and the reconstruction of petroleum inclusions exhibit remarkable similarity, with a high degree of resemblance observed between the calculated phase envelopes (Fig. 11). Similarly, by adjusting the parameters mentioned above, the output compositions from different geological periods are consistent with the petroleum inclusions. The validity of the output results is evaluated by analyzing the correlation coefficients between the normalized components of both datasets. With constraints from various parameters, it is believed that the reconstructed deep condensate gas phase evolution by this method is credible.

4.3.2. *Hydrocarbon phase evolution*

In this study, the fluid phase evolution of deep condensate gas reservoirs was reconstructed based on the hydrocarbon generation history and structural evolution history, focusing on the phase behaviors during petroleum migration and charging. The simulation results at each evolutionary period are as follows.

(1) ~39Ma to 36.8Ma: During the subsidence period, the majority of mudstones in the Es_4 reached the oil window, leading to the generation of liquid petroleum. Additionally, natural gas generation occurred at depths exceeding 4000m. Oil charged into adjacent sandstone reservoirs and migrated towards the shallow parts of the sandstone fan body under buoyancy (Fig. 12a). The gas migration in the sand body was forced by overpressure and buoyancy (Fig. 12a). However, the upward migration range was limited and did not reach the simulated reservoir. Hydrocarbons in the simulated reservoir remained a liquid phase (Fig. 11b). During this period, the changes in phase envelopes and the movement of critical points indicate an increase in light components due to enhanced maturity (Fig. 12b). The molar content of CH_4 increased by ~10% but cannot induce a hydrocarbon fluid phase transition (Fig. 11a and b).

(2) ~24.4Ma: The strata reached the maximum burial depth during this period. The source rocks of the lower part of the Es_4 generated oil and gas ($R_o > 1.0\%$). Meanwhile, a substantial volume of natural gas migrated upward, progressively filling the traps by

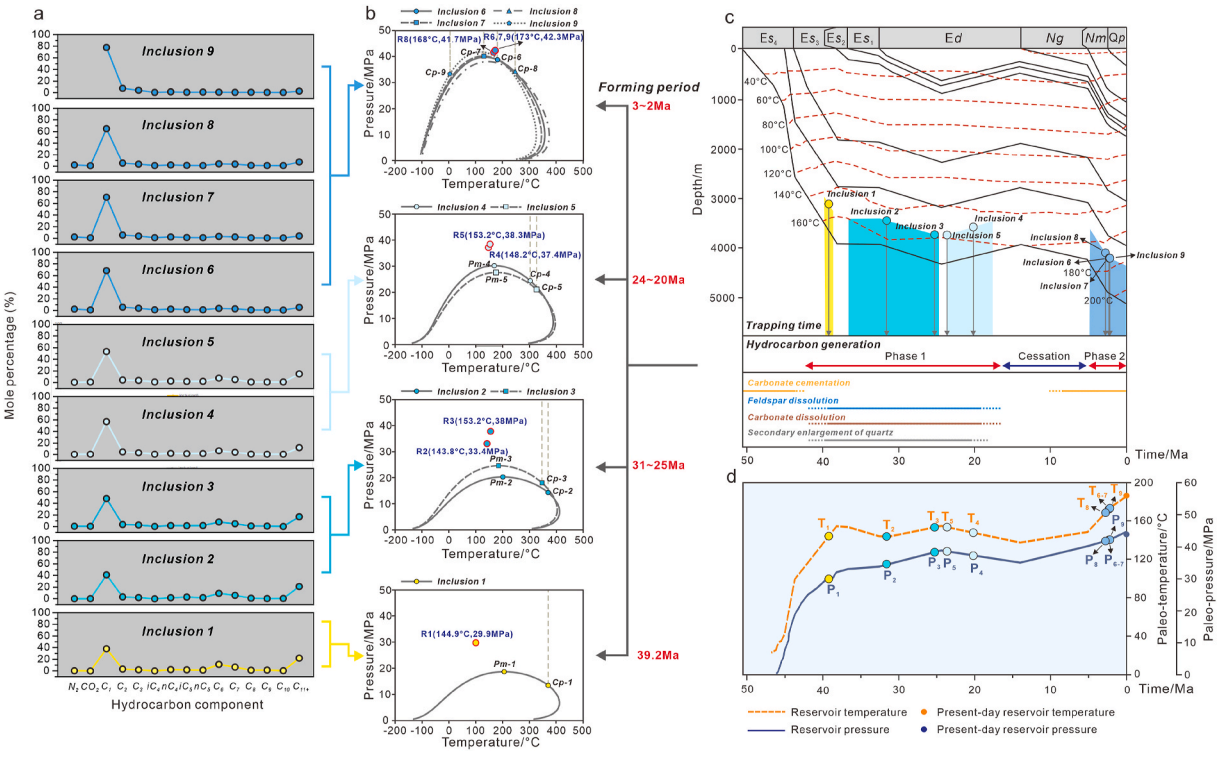

Fig. 9. Hydrocarbon compositions, phase envelopes, trapping time, and trapping temperature-pressure conditions of oil inclusions from the condensate gas reservoir reconstructed by petroleum inclusion thermodynamics and basin modeling. (a) The molar fraction of the petroleum components of each measured inclusion. The different colors indicate the fluorescent color of the corresponding inclusions. (b) The phase envelopes and critical points of petroleum inclusions with different fluorescent colors. The phase state of the hydrocarbon fluid was determined by combining the temperature-pressure condition and the phase diagram when the inclusion was trapped. The R1-R9 points indicate the reservoir conditions during the formation of inclusion 1–8. The Cp-1 and Pm-1 represent the critical point and the cricondenbar of the inclusion 1, respectively. (c) The burial and thermal histories of well FS1, showing the trapping time of the petroleum inclusions. (d) The formation temperature and pressure evolution line for the determination of the paleo reservoir conditions when the petroleum inclusions were formed.

Table 7
Hydrocarbon components derived from petroleum inclusions in molar fraction (Mol, %).

Component	Inclusion 1	Inclusion 2	Inclusion 3	Inclusion 4	Inclusion 5	Inclusion 6	Inclusion 7	Inclusion 8	Inclusion 9
N_2	0.5	0.6	0.7	0.8	0.7	2.3	2.3	2.2	
CO_2	0.6	0.7	0.8	0.9	0.9	0.7	0.8	0.7	
C_1	38.5	41.3	48.4	56.9	52.9	68.4	70.4	64.9	77.6
C_2	3.5	3.7	4.2	4.8	4.5	5.4	5.5	5.1	7.6
C_3	3.0	3.0	3.2	3.4	3.3	3.7	3.8	3.6	4.0
iC_4	1.0	1.0	1.0	1.0	1.0	1.1	1.1	1.0	0.7
nC_4	2.8	2.5	2.5	2.4	2.4	2.2	2.2	2.1	1.5
iC_5	2.5	2.3	2.1	1.8	1.9	1.2	1.2	1.2	0.8
nC_5	2.9	2.5	2.3	2.0	2.1	1.1	1.1	1.1	1.2
C_6	11.1	10.0	8.5	6.7	7.5	3.5	3.3	4.0	1.0
C_7	7.1	6.6	5.5	4.1	4.8	2.8	2.4	3.5	1.0
C_8	1.7	1.7	1.4	1.0	1.2	0.9	0.7	1.2	0.8
C_9	1.3	1.4	1.1	0.8	1.0	0.8	0.6	1.1	0.7
C_{10}	1.1	1.3	1.1	0.8	0.9	0.7	0.5	0.9	0.6
C_{11+}	22.4	21.4	17.4	12.6	14.9	5.2	4.0	7.3	2.5

steps. The mixing of oil and gas in these traps resulted in the formation of gas caps in some of the early-formed oil reservoirs (Fig. 12c). During this period, most of the mudstones continued to expel liquid hydrocarbons into adjacent traps, where liquid hydrocarbons were accumulating in traps at depths greater than 4000 m. The petroleum in the simulated reservoir remained in the liquid phase, with an increase of gaseous hydrocarbons, exhibiting characteristics of light oil (Fig. 12d). This indicates that as maturity increases, the components of the liquid hydrocarbons become lighter.

(3) ~14Ma: The overall uplift and erosion induced a weakening or cessation of hydrocarbon generation. The release of overlying stress increased the pressure difference between the source rock and reservoir, driving the retained oil and gas expulsion and migration. Meanwhile, the uplift event also led to the expansion of gas vertical migration range (Fig. 12e). The phase envelope of the simulated reservoir is similar to that at 24.4 Ma. The reduced formation pressure is close to the bubble point curve (Fig. 12f)

(4) ~5Ma to 0Ma: The Dongying Depression underwent the second subsidence. The transition from liquid phase to gas phase can be observed in the simulated reservoir by comparing the phase diagrams in Fig. 12h with Fig. 12j. After 5Ma, natural gas migrated along the stacked sand bodies to the simulated interval. Meanwhile, the ability of source rocks to generate liquid hydrocarbons

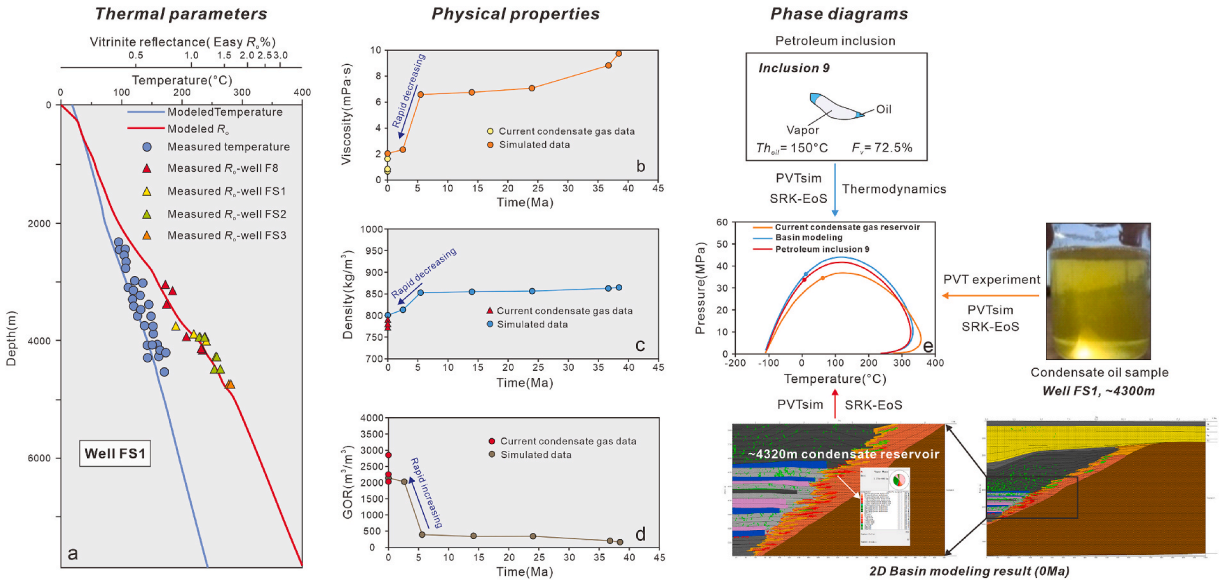

Fig. 10. Calibration of the 2D basin model from thermal parameters, petroleum physical properties, and phase diagram. (a) The measured temperatures and vitrinite reflectance values were used to correct the modeled curves of well FS1. Some thermal data was derived from nearby wells F8 and FS2. The location of well FS1 is shown in Fig. 4. The evolutions of viscosity (b), density (c), and GOR (d) in the deep condensate gas reservoir at the depth of ~4320m, showing a good match with the measured data of the current condensate gas reservoir. (e) The phase envelopes reconstructed by petroleum inclusions, PVT experiment for the condensate oil sample and 2D basin modeling, indicating that the 2D basin model can generate a reasonable result for phase evolution.

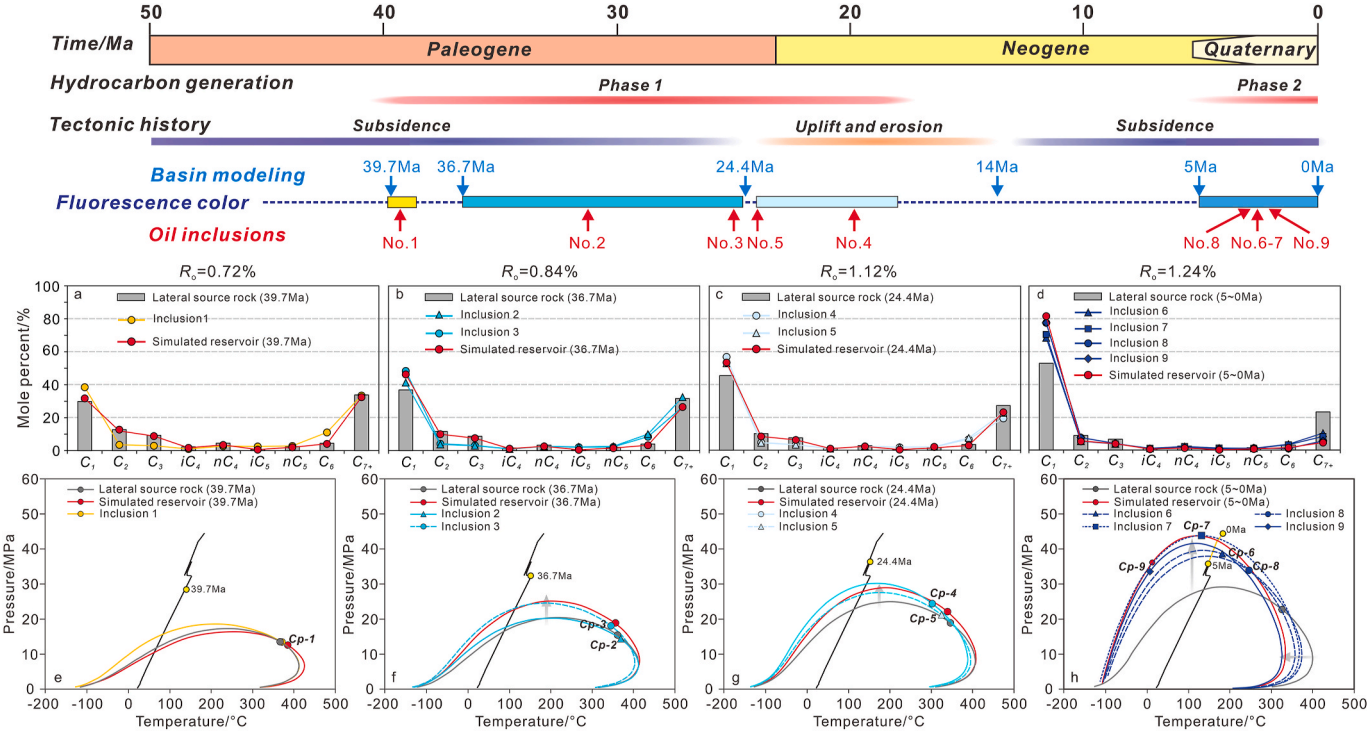

Fig. 11. Component distribution and phase diagrams of the simulated oil and gas reservoir, generation products from lateral source rock, and petroleum inclusions at different geological times.

diminished (Fig. 12g and i). The phase envelope lines significantly shifted to the left, with a rapid decrease in critical temperature and pressure, indicating a substantial increase of gaseous hydrocarbon. At present, the temperature and pressure of the simulated reservoir surpass the critical condition, which confirms the condensate gas accumulation (Fig. 12j).

5. Discussion

5.1. Control of hydrocarbon generation on the phase state of trapped oil and gas

The trap-filling model indicates that oil and gas will migrate laterally and be charged into the neighboring traps (Fig. 4). The distribution of hydrocarbon phases may be controlled by the degree of thermal

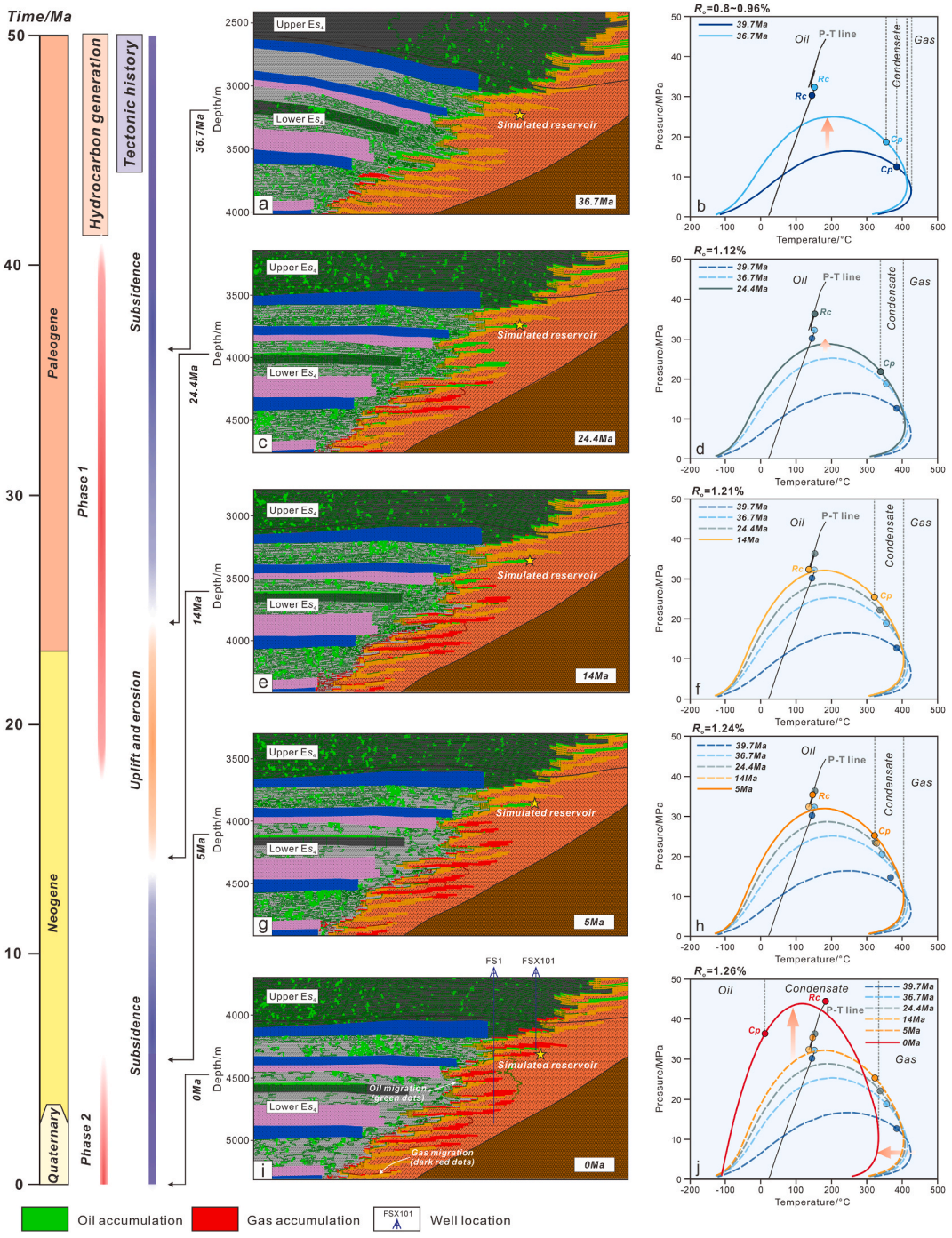

Fig. 12. Fluid phase evolution of the deep condensate gas reservoir, showing the petroleum migration and accumulation during the geological periods of (a) 36.7 Ma, (c) 24.4 Ma, (e) 14 Ma, (g) 5 Ma, and (i) 0 Ma. The temperature-pressure conditions, phase envelopes, and corresponding critical points of the fluids in the simulated reservoir at (b) ~39.7 Ma, 38.6 Ma, 36.7 Ma, (d) 24.4 Ma, (f) 14 Ma, (h) 5Ma, (g) 2 Ma and 0 Ma. The phase states of different times can be determined by the phase diagrams. The Cp indicates the critical temperature and critical pressure. The Rc point represents reservoir temperature and pressure of the simulated reservoir.

evolution of the lateral source rocks, because the plane distribution of well types in the study area shows a sequence from dry gas wells, condensate wells to oil wells, from the center to the north of the Minfeng Sag (Fig. 1). Hydrocarbons produced from the reservoirs discovered near the center of sag are predominantly of high maturity stages. For example, dry gas and condensate were found in deep sandstone reservoirs by wells FS3 and FS1, respectively (Figs. 1 and 13a). Different petroleum phases exhibit a vertical distribution, with oil mainly produced in the reservoirs at depths greater than 4300m, condensate gas predominantly accumulating in the sandstones buried at depths of 4300–4500m, and dry gas being discovered in the formations deeper than 4700m (Figs. 2 and 13a). Theory of kerogen thermal degradation explains the transformation of kerogen into different phase hydrocarbons at various thermal evolution stages (Tissot and Welte, 1984). Typically, the primary product of organic matter at maturity stages is liquid petroleum, corresponding to vitrinite reflectance (R_o) ranging from 0.5% to 1.3%. When organic matter reaches high maturity stages (R_o = 1.3% ~ 2.0%), kerogen degrades to form short-chain hydrocarbons, while liquid hydrocarbons are cracked to form low molecular weight gaseous hydrocarbons. The main products at this stage are wet

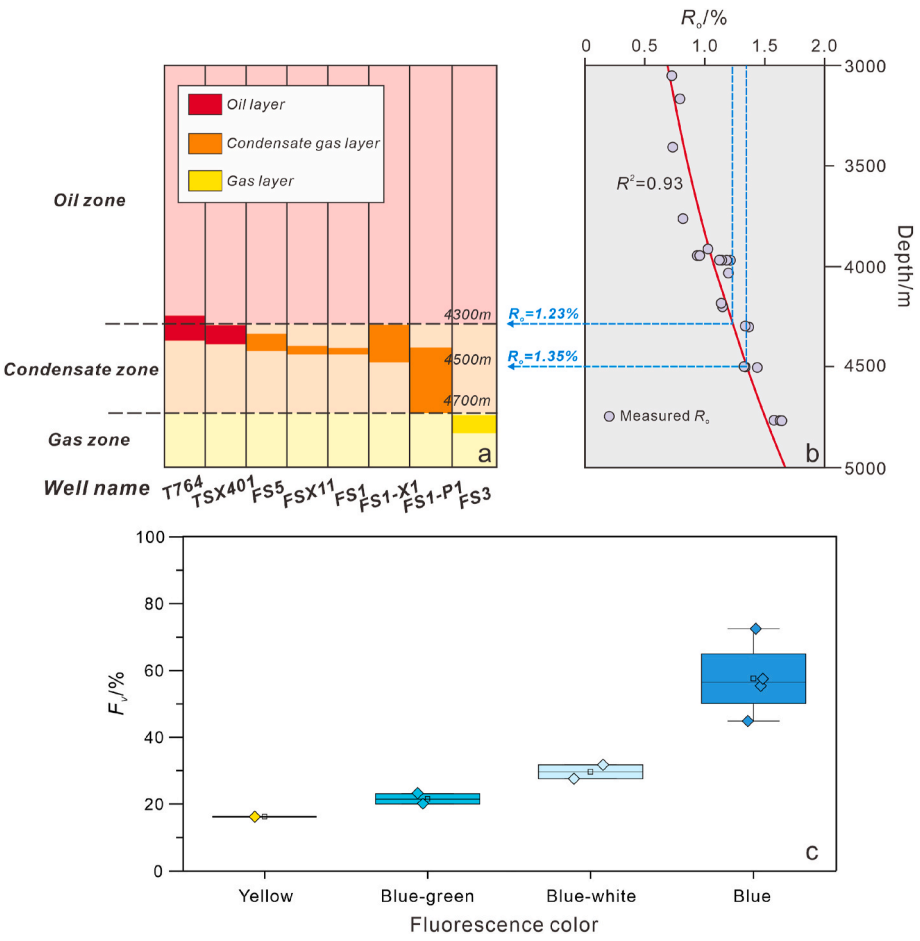

Fig. 13. (a) Vertical distribution of hydrocarbon phase states in the deep reservoirs (modified from Qiao et al., 2022). (b) The relationship between the measured vitrinite reflectance and burial depth. The measured R_o points are same as those presented in Fig. 10a. (c) The gas filling degrees of petroleum inclusions with different fluorescence colors.

gas or condensate gas. At over-mature stages (R_o > 2.0%), liquid hydrocarbons and heavy gaseous hydrocarbons undergo intense decomposition to form methane gas, i.e., dry gas. This indicates that the maturity parameter (R_o) or burial depth can be used to predict the phase of hydrocarbons generated from kerogen. Therefore, based on the relationship between the measured R_o and burial depth in the region, the calculated R_o range for the condensate gas pools was 1.23%–1.35% (Fig. 13b), which is similar to the thermal maturity obtained from basin modeling, with R_o approximately equal to 1.26% (Fig. 12j). According to the kerogen thermal degradation theory, the source rocks should be in the oil window. However, condensate gas is enriched in the adjacent reservoirs. Additionally, wells T764 and TSX401 in the Dongying Depression encountered oil reservoirs at similar depths, suggesting that the condensate gas found in the region is not directly sourced from the lateral mudstones. (Fig. 13a).

The oil inclusions in the reservoirs recorded information about the maturity, composition, and PVT characteristics of hydrocarbon products, which can be used to infer the characteristics of hydrocarbon fluids during the trapping period. The fluorescent color of liquid hydrocarbons is primarily determined by the aromatic hydrocarbon conjugated π-bond system and the C=O functional group (Van Duuren, 1960; Fu et al., 2015). Therefore, the cracking of aromatics during thermal evolution leads to changes in fluorescence color. The oils transition in fluorescent colors from red to yellow, green, blue-white, and blue as organic matter matures, accompanied by changes in the proportion of light and heavy components (George et al., 2001). Petroleum inclusions in deep condensate gas reservoirs show a variety of fluorescence colors (Fig. 7). As the gaseous hydrocarbon components, mainly methane, increased, the fluorescence color of fluid inclusions transitioned from yellow to blue (Fig. 9a). Additionally, the relationship between the gas-liquid volume ratio and the fluorescence color of petroleum inclusions indicates the response of aromatics cracking into gaseous hydrocarbons during thermal evolution (Fig. 13c). The phase diagrams of oil inclusions indicate the trapped fluids at different evolutionary stages, ranging from early heavy oil to late light oil and condensate gas, which confirms the charges of these fluids (Fig. 9b). Further comparison of the trapped oils and gases at different times with the products generated from lateral source rocks was conducted to analyze the control of hydrocarbon generation on fluid phase states. The hydrocarbon components and phase envelopes of oils generated by early mature source rocks (~39.7Ma) are similar to those trapped by contemporaneous fluid inclusions at the same time (Fig. 11e). As the source rocks enter the main oil generation stage (~36.7Ma) equal to Ro = 0.7–1.0%, the hydrocarbon components and the phase diagrams of inclusion 2 closely resemble the generated petroleum (Fig. 11f). This indicates that the hydrocarbons generated by source rocks largely determine the petroleum phase state during the early stage. The basin modeling also shows that the oil and gas in the traps during this period mainly came from adjacent source rocks (Fig. 12a). The physical properties of deep sandstone reservoirs vary rapidly in the vertical direction. The sedimentary interfaces of fan deposits, muddy conglomerates of the proximal fan, and mudstone interlayers can act as low-permeability barriers to hydrocarbon migration (Song et al., 2019; Yang et al., 2023). The heterogeneity of sealing causes some reservoirs can accumulate hydrocarbons with higher maturity from the deeper source rocks. For instance, the oil trapped by inclusion 3 has a methane content approximately 10% higher than the

oil generated from the lateral source rocks, leading to an upward shift in the phase envelope (Fig. 11f). In the late stage of main oil window (~24.4Ma), the hydrocarbon components in the fluid inclusions still maintain a characteristic of methane molar percentage approximately 10% higher than the hydrocarbons from source rocks (Fig. 11g). Guo et al. (2020) utilized in-situ U-Pb dating by laser ablation to analyze the calcite veins in deep mudstones, confirming that around 24Ma was the main hydrocarbon accumulation period in the Dongying Depression. The allowed relatively high mature hydrocarbons to steadily migrate and accumulate vertically (Fig. 12). Additionally, the biomarker compounds demonstrated that the shallow oil in structural reservoirs originated from the lower part of the Es_4 source rocks, further confirming the vertical migration of deep hydrocarbons (Song et al., 2021). The simulation results show that a large-scale vertical migration of oil occurred in the stacked traps during this period. Furthermore, some traps accumulated gas in the deeper region with high maturity (Fig. 12c). During the second hydrocarbon generation period following the uplift and erosion event, the phase envelopes of the included petroleum represent distinct differences from those of the lateral mudstone sourced hydrocarbons, showing a significant leftward shrinkage and upward shift. This indicates a sharp increase in CH_4 content and a decrease in heavy hydrocarbons of petroleum (Fig. 11h). Meanwhile, between 5 ~ 0Ma, the simulated reservoir was charged by gaseous hydrocarbons and became a condensate gas pool (Fig. 12i). Therefore, the phase states of deep oil and gas are related to gas migration and charging, as well as other geological processes that can lead to an increase in gaseous hydrocarbons. The hydrocarbon generation influenced the early phase state of deep oil and gas, providing initial hydrocarbon components for the entire evolution. In the deep carbonate rocks of the Leikoupo Formation in the Sichuan Basin, native condensate gas pools have been discovered, which are sourced from the neighboring mudstones (Zhu et al., 2011). Nevertheless, it is difficult for native condensate gas to exist in reservoirs with good vertical connectivity.

5.2. Effect of secondary alteration on petroleum phase evolution

The difference in hydrocarbon composition between the included petroleum and the hydrocarbons from the lateral source rocks reveals a crucial phase transition. During a subsequent hydrocarbon generation (~5Ma), the fluid inclusions recorded a large increase in methane content with a decrease in heavier hydrocarbon components (Fig. 11d and h). Moreover, the temperature and pressure conditions resemble those around 24.4Ma (Fig. 9d). Constrained by the reservoir conditions, these compositional changes directly result in a shift from oil reservoir to a gas-capped reservoir (Fig. 12h). As temperature and pressure continue to rise, the deep oil and gas transition into either condensate gas or undersaturated light oil (Fig. 12j). Meanwhile, the trends in viscosity, density, and GOR indicate that the oils were lightning during the late period (Fig. 10b, c, d). Therefore, the primary factor driving the petroleum phase transition is the increase in gaseous hydrocarbon components, particularly methane. The variation in methane molar percentage mainly affects the cricondenbar, thereby controlling the phase behaviors of oil and gas (Di Primio et al., 1998). Indeed, the fundamental cause of the changes in hydrocarbon components is the modification of reservoir fluids by relevant geological processes, that is, secondary alteration, such as cracking of crude oil and gas inputs.

5.2.1. Oil cracking

Oil cracking is a process in which higher-numbered components in crude oil are broken down into lower-numbered components under high temperatures (Hill et al., 2003). The analysis of maturity suggests that the current depth of 4300–4500m corresponds to the R_o values of less than 1.3%, which is below the threshold for oil cracking. Measurements from three wells indicate current condensate reservoir temperatures of 165–185 °C (Table 3), all exceeding 160 °C as a threshold temperature for oil cracking in the Dongying Depression (Li et al., 2010). Qiao et al. (2022) considered that overpressure in the Es_4 and the deposited evaporites can restrain maturation in hydrocarbon source rock of the Dongying Depression, resulting in lower vitrinite reflectance than expected for normal evolution (Mello et al., 1995). However, the temperature of sandstone reservoirs remained unaffected, leading to a contradiction in the above inference. Consequently, it is inferred that the deep paleo-oil pools underwent cracking at this formation temperature. The pyrobitumen observed under the microscope further confirms the occurrence of crude oil cracking (Liu et al., 2012). Generally, the increase in volume induced by oil cracking will result in overpressures in the pores under closed conditions. However, Ping et al. (2017) found that the trapping pressure of fluid inclusions in the condensate reservoir of well FS1 equaled hydrostatic pressure, indicating that the reservoirs maintained normal pressure throughout the entire period of oil and gas charging. Additionally, even under a closed reservoir condition, the formation of overpressure during oil cracking is related to the extent of the cracking. Ping et al. (2014) suggested that a sharp increase in formation pressure induced by oil cracking, typically requiring a conversion rate of oil cracking of over 40%. Therefore, it is inferred that the extent of oil cracking in the investigated zone is less than 40% or even lower. Furthermore, the conversion rate of oil cracking (R_{oc}) in the deep petroleum reservoirs from the onset of the second phase of subsidence (~14Ma) to the present was calculated based on basin modeling results using the following formula:

$$R_{oc} = \frac{MI_{C6+} - MR_{C6+}}{MI_{C6+}} \quad (1)$$

where R_{oc} is the conversion rate of oil cracking, namely the fraction of the oil that has been cracked to gas. MI_{C6+} is the mass of C_{6+} liquid hydrocarbons before cracking, and MR_{C6+} indicates the remaining mass of C_{6+} liquid hydrocarbons during oil cracking.

The simulated migration pathways indicate that the charge of natural gas into the reservoirs of the target zone occurred after 5Ma (Fig. 12g–i). Throughout the entire charging period, the petroleum inclusions suggest that the hydrocarbons in the deep condensate reservoirs originate from the mixing of two parts: (1) hydrocarbons generated from the neighboring source rocks and (2) deeper oil and gas with relatively higher maturity (Fig. 11e and f). The mixing of hydrocarbons with varying maturities will complicate the calculation of the mass of cracked oil during migration and accumulation. Therefore, in this study, the interference from the mixing was eliminated in the model by assigning kinetic parameters of hydrocarbon generation only to the lateral source rocks. This model aimed to obtain the oil mass before and after cracking and to calculate the conversion rate of oil cracking. According to compositional kinetic models, the oil cracking process can be described by parallel first-order reactions (Del Bianco et al., 1993). The rate constants of the chemical reaction follow the Arrhenius equation, indicating that the oil cracking conversion rate is a function of temperature and time (Ungerer et al., 1988). Consequently, the adjusted basin model can reflect the extent of oil cracking during the evolutionary stages. The burial depth range of the present deep condensate gas reservoirs is 4300–4500m. Simulating the oil cracking processes in the shallowest and deepest reservoirs can determine the variation range of the R_{oc}, allowing an assessment of the impact of oil cracking on mole fractions of components and phase behavior. Fig. 14c illustrates that the crude oil cracking rate in the paleo-oil pools ranges between 2.21% and 8.72%, indicating a relatively low degree of cracking and an early stage of thermal cracking. Qiao et al. (2022) found that the absolute content of 3- + 4-methyldiamantan as a thermal cracking indicator in the condensate is 39.27×10^{-6}, indicating a low oil cracking conversion rate. During the cracking of C_{6+} liquid hydrocarbons, the methane mole fraction increased by 3.81%–11.58% and $C_{2\text{-}5}$ gaseous hydrocarbons reduced by 1.53%–3.92%, suggesting that the primary cracking product is methane (Fig. 14a and b). Furthermore, from Fig. 14a, it can be observed that the methane mole fraction comprises approximately 50%

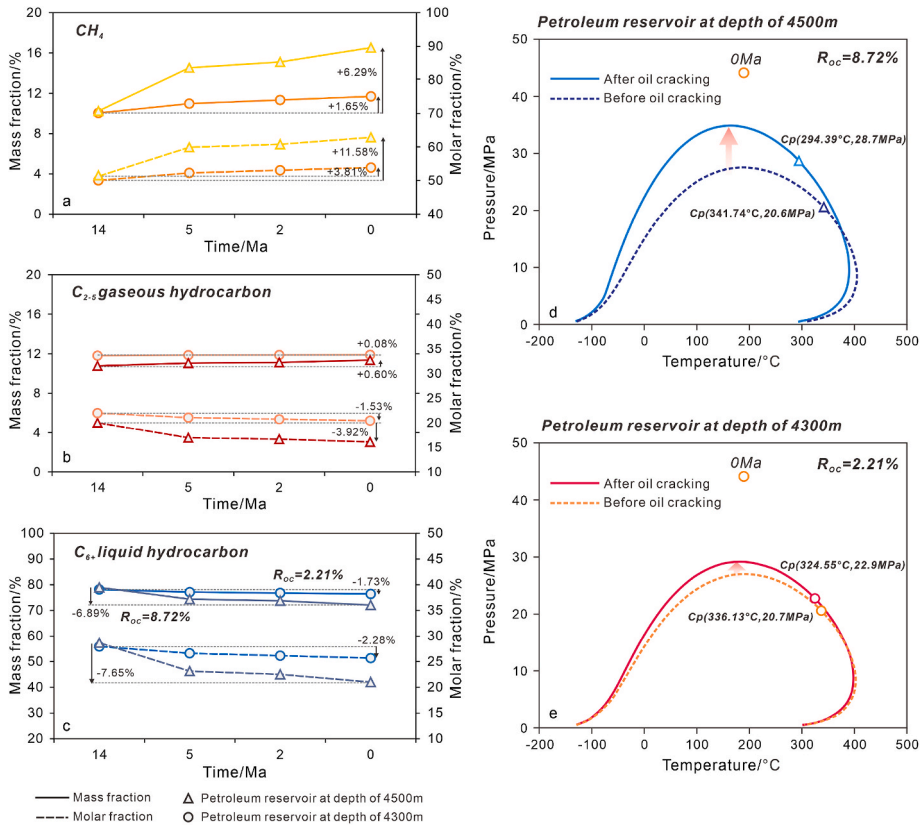

Fig. 14. (a–c) The changes in the mass fraction and molar fraction of different hydrocarbon components in the two reservoirs, during the process of oil cracking. (d–e) The phase diagrams of the petroleum in the two reservoirs before and after oil cracking. The present burial depth of one petroleum reservoir is 4300m, while the present burial depth of another is 4500m.

of the petroleum before oil cracking. The oil cracking simulation shows that the methane mole fraction increases to around 60%, representing a difference of 10%–20% compared to the present-day condensate (Fig. 14a, Table 5). This indicates that methane generated from in-situ cracking can increase the cricondenbar but is insufficient to induce phase change, with the hydrocarbon fluids remaining in the liquid phase (Fig. 14d and e). Therefore, the impact of in-situ oil cracking in the Dongying Depression on the overall phase evolution is limited, which is closely related to formation temperature. Oil cracking can increase the methane mole fraction in paleo-oil pools by approximately 4%–12%.

5.2.2. Gas inputs

Reservoir petroleum can receive successive charges of gas from deeper zones, leading to the enrichment of methane gas in the oils (Thiéry et al., 2002). Analysis of the oil cracking indicates that the in-situ oil cracking is unable to form condensate gas. Therefore, the external gaseous hydrocarbon inputs may be the key factor leading to the phase change in deep reservoirs. The discussion in Section 5.1 revealed the presence of vertical migration pathways in the overlapping fan bodies. Fig. 2 shows that the thickness of the mudstones in the lower part of the Es_4 is large. Some mudstones are currently buried at depths exceeding 5000m and reach the high-over mature stage with $R_o > 1.6\%$ (Fig. 13a). The deeper sandstones are enriched with natural gas formed by early kerogen degradation and late oil cracking. The molecular diameter of gas is relatively smaller than that of oil, making it prone to migration and diffusion in sandstones (Stainforth and Reinders, 1990). Additionally, the observation of amorphous asphaltene in thin sections is believed to be formed by gas invasion into the oils (Liu et al., 2012). After the gas is charged into an oil pool, volatile components are extracted by the methane gas. The low-carbon-number normal alkanes will be lost when the gases escape. This means that evaporative fractionation selectively depletes light components in the oil. Qiao et al. (2022) reported the losses of $C_5 \sim C_{10}$ normal alkanes in the deep condensate. Ping et al. (2017) considered that the gas was injected into the deep paleo-oil and remained dissolved in the oils. To sum up, abundant natural gas with high maturity has been charged into the early paleo-oil reservoirs.

The basin modeling indicates that the major gas injection to the simulated reservoir occurred after 5Ma (Fig. 12i and j). Petroleum inclusions also reveal a marked increase in CH_4 content after the second subsidence event, accompanied by a decrease in heavy hydrocarbon content (Fig. 9a). A comparison between Figs. 12c and i illustrates that the strata were buried deeper and the temperatures were higher during the second subsidence event. It is generally believed that when the oil cracking conversion rate exceeds 62.5%, the liquid phase will completely disappear. Modeling results suggest that the oil cracking conversion rate in the deeper zone reached 70%, which can provide plenty of natural gas. Moreover, the extra fluid pressure generated by oil cracking to gas can drive the vertical migration of these gases when the overpressures release towards shallower strata. This process will increase the efficiency of gas migration and charging to upper reservoirs. The contributions to accumulated hydrocarbon components of the lateral source rocks and the deeper source rocks were revealed by the basin modeling. From 14 Ma to 5 Ma, the molar fraction ratio of hydrocarbons from deeper and lateral source rocks was approximately 1:1 (Fig. 15a and b). After 5 Ma, the proportion of methane generated from the deeper zone in the reservoir hydrocarbons increased by ~50%, resulting in an overall methane molar fraction increase to ~80% (Fig. 15a). The contribution ratio of deep-sourced gas exceeded 90% (Fig. 15b). Therefore, the influx of methane led to the late-stage transformation from the oil phase to the condensate gas phase (Fig. 12 g, i). The deep light oil reservoir encountered in Well T764 is located at a

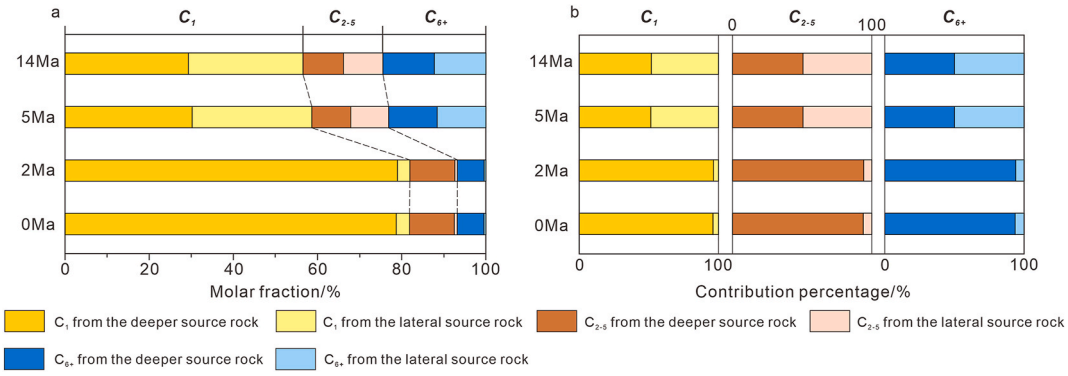

Fig. 15. (a) Molar fraction of the components of the hydrocarbons derived from the deeper and lateral source rock at different periods. (b) Contribution percentage of the deeper source rocks and the lateral source rocks to C_1, C_{2-5}, and C_{6+} at different periods. The hydrocarbon compositions from the simulated reservoir at the burial depth of ~4320m (Fig. 12).

depth similar to these condensate reservoirs but exhibits a different phase state. The light oil of Well T764 is accumulated within sandstone lenses enclosed by mudstones, resulting in a lack of migration pathways for external natural gas. In this region, relying solely on the gas produced by in-situ oil cracking is insufficient to alter the phase state. This further demonstrates the importance of external gas injection for condensate gas formation in the Dongying Depression.

Petroleum accumulated in the investigated reservoir at 24 Ma was chosen to investigate the phase behaviors when these oils were mixed with the late deeper gases at varying molar ratios. As the gas mole fraction increases, the critical temperature and cricondentherm gradually decrease, and the critical pressure and cricondenbar initially increase and then decrease (Fig. 16). Under a high-temperature and high-pressure environment (44 MPa, 175 °C), the molar fraction of deeper natural gas needs to exceed 50% to form a condensate gas reservoir (Fig. 16). This is equivalent to 0.8 m^3 of gas per 1 m^3 of oil under the reservoir condition. Hydrocarbon fluid inclusions at a burial depth (~4500 m) in well FSX101 exhibit different phase behaviors. When deeper gas constitutes 70% of the mixture, the phase diagram resembles that of inclusion 7, indicating the presence of condensate gas. Furthermore, the phase diagrams of inclusions 6 and 8 show similarities to those of the petroleum with deeper gas molar fractions of 30% and 50%, respectively, displaying characteristics of light oil (Figs. 16 and 11h). At 5 Ma, the oil-gas two-phase system exists in the trap with the current burial depth of 4500 m (Fig. 12g). The trapping timing of hydrocarbon fluid inclusions is approximately 3 Ma (Fig. 9c). The phenomenon of different phase fluids being trapped during the same period may suggest a process of phase transformation induced by secondary alterations.

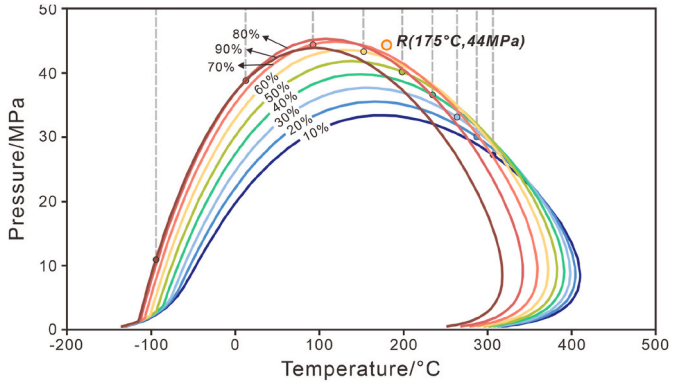

Fig. 16. Phase behavior of the early oil mixed with late deeper gas at different molar ratios. The percentage on the envelope indicates the mole fraction of the deeper gas after mixing. The circle R indicates the present-day reservoir temperature and pressure.

5.3. Formation model of deep condensate gas reservoir

The deep condensate gas reservoirs in the Dongying Depression are the result of thermal evolution and gas inputs. The vertical distribution of oil and gas in stacked reservoirs is affected by (preferential) vertical migration and leaking of gas. Furthermore, the deep condensates are mainly developed at depths of 4200–4500m, indicating a limited range of gas migration towards shallower formations (Fig. 13a). Basin modeling indicates a stepwise occurrence of gas invasion in traps, transitioning from deeper to shallower levels. The upward migration of natural gas is confined to approximately 4000 m. This study suggests that such successive lithologic traps control the range of deeper gas migration and the occurrence of condensate gas (Fig. 17). The model illustrates the various stages of oil and gas accumulation in these traps. Moreover, the calculated oil cracking conversion rates of the reservoirs at different period reveal the contributions of cracking gas and external deep gas to the hydrocarbon phase changes.

In the early stages, as the source rocks mature, the crude oil migrated under buoyancy and accumulated in the traps (Fig. 17a). Natural gas generated from source rocks and oil cracking accumulated in the deeper zone, with some gas migrating to the upper reservoirs. The oil cracking rate in the charged reservoirs was low, and the influx of external gas formed gas caps (Fig. 17a). The oil phase was maintained in the simulated reservoir (Fig. 17e). Continued burial led to an increased thermal evolution in the deeper zone, resulting in a rapid increase of gas content and volume in the traps (~24.4 Ma) (Fig. 17b). For a gas reservoir, when the fluid volume exceeded the capacity of the trap, gas components will escape from the spill point (Fig. 17b). During this process, natural gas will be injected into the oil reservoirs, dissolving in the oils and gradually inducing a phase change. During this period, the oils in the simulated reservoir lightened due to increased thermal maturation (Fig. 17f). In the uplift and erosion event, a part of gases from the deeper zone was injected in the upper liquid oils, forming oil reservoirs with gas caps (Fig. 17c). The decrease of reservoir temperature and pressure did not affect the phase state of deep oil and gas (Fig. 17g). It is found that the oil cracking rate in reservoirs affected by gas invasion is relatively low, resulting in the onset of significant oil cracking occurring later than the natural gas injection (Fig. 17a, b, c, d). This leads to gas inputs dominating the evolution of hydrocarbon phase behavior. Meanwhile, the dissolved oil components in the condensate gas can crack to gaseous hydrocarbons. From 5 to 0 Ma, the degree of oil cracking in the early-formed condensate gas reservoirs increased, releasing a substantial amount of natural gas. The simulated oil reservoir subjected to gas invasion gradually transition into condensate gas reservoir (Fig. 17h).

The basin modeling reveals the gas input and subsequent spilling (Fig. 12), which will lead to three results: (1) a gradual consumption of the gas generated from deeper zone due to dissolution; (2) a loss of light hydrocarbons from the oil reservoirs; (3) an orderly petroleum fluid

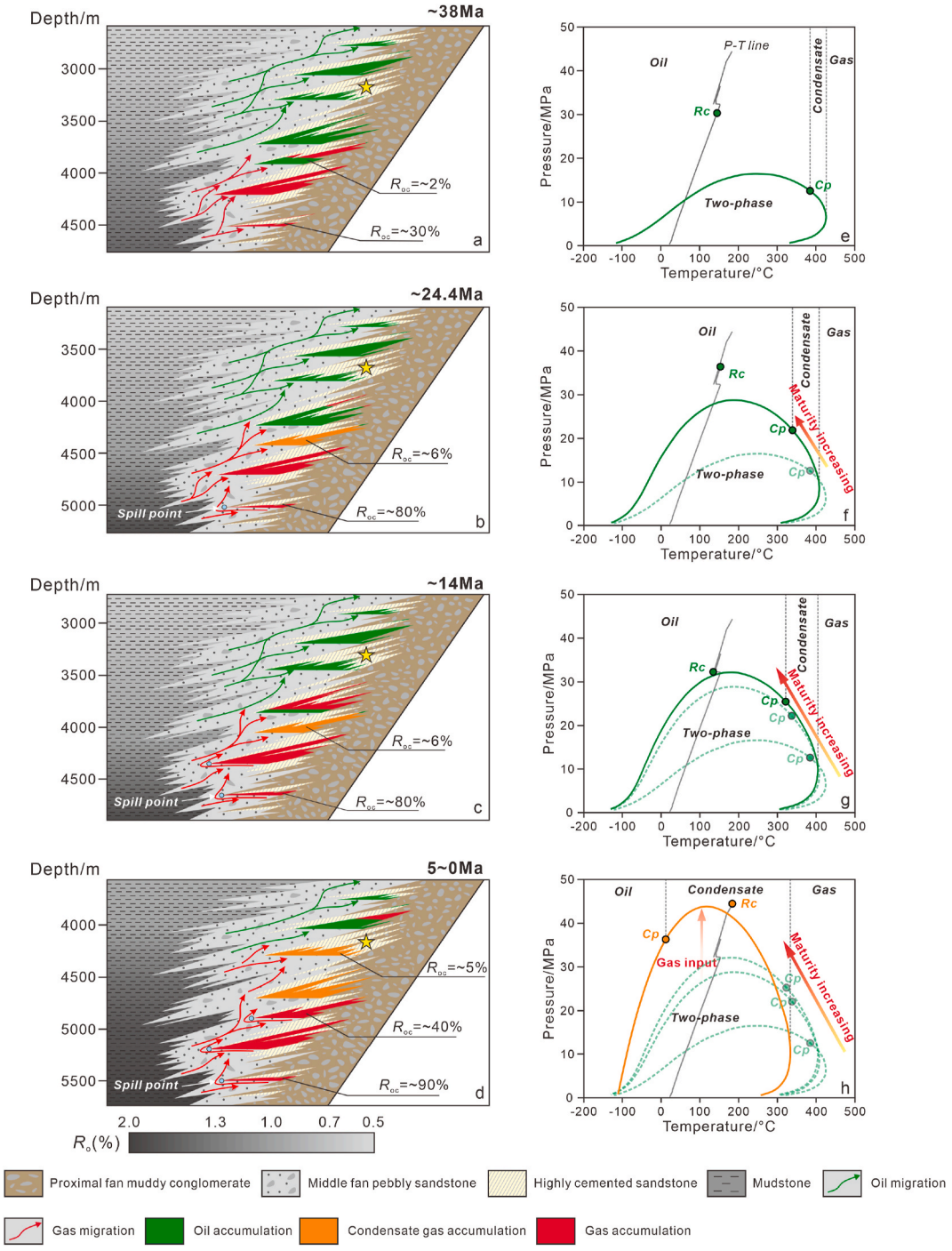

Fig. 17. Formation model of the deep condensate gas in the Dongying Depression. This model was constructed based on basin modeling and phase evolution, which explains how the stacked lithological traps control the deep gas migration range and the accumulation of condensate gas. The yellow star indicates the simulated reservoir for phase analysis. The Cp indicates the critical temperature and critical pressure. The Rc point represents temperature and pressure in the simulated reservoir.

phase changes in the deep reservoirs in a vertical direction. Due to the limited amount of gas from the deeper zone, it cannot migrate to shallower formations after successive charging and consumption (Fig. 17d). Therefore, these light oils can be preserved and accumulated in the sandstone above the condensate gas reservoirs. The formation of light oil reservoirs also involves the gas inputs, where the molar fraction of the deeper gas is relatively low, around 20%–40% (Fig. 15). In addition, the practical exploration discovered only liquid oil accumulations with no gas reservoirs in the shallow strata in the region, which is sourced from the mudstones of the lower part of the Es_4 (Song et al., 2021). These shallow oil pools indicate the significant consumption of deeper natural gas during this process. Thus, the condensate gas accumulations indicate the farthest distance to which the deeper gas can be supplied upwards.

6. Conclusions

The reconstruction of fluid phase evolution in deep condensate gas reservoirs in the Dongying Depression was achieved through a combination of methods involving petroleum inclusion analysis, basin modeling, and PVT simulation. The analysis of the fluid phase evolution

in deep condensate gas reservoirs revealed several key points.

(1) The fluid phase evolution in the deep condensate gas reservoirs of the Dongying Depression can be divided into three main stages. The crude oil charging and accumulation period (38–14 Ma). The in-situ oil cracking period (14–0 Ma). The external gas influx period (5–0 Ma). The hydrocarbon generation provides the initial hydrocarbon components for the phase evolution. The in-situ oil cracking has a limited impact on components. Gas inputs dominate the alteration of the hydrocarbon physical properties with a reduction in critical temperature and pressure, forming the present-day condensate gas reservoirs under high pressure and temperature conditions.
(2) Hydrocarbon inclusions record the components, temperatures, and pressures during the trapping periods, which can be used to calibrate the phase states on the timeline. These phase states have strong constraints on basin modeling results. Additionally, the diversity of hydrocarbons trapped during the same period can reflect the different phase transitions in the same reservoir, documenting the intermediate phase states during evolution. Meanwhile, the high-pressure physical property parameters of wellstream fluids serve as reliable constraints for basin modeling.
(3) The stacked lithologic traps developed in the Dongying Depression in succession control the range of deeper gas charging towards the upper traps and hydrocarbon phase distribution. The model aids in understanding the mechanism of orderly phase changes in deep oil and gas, from oil phase to condensate phase, and ultimately to gas phase.

Although the method reconstructed the deep petroleum phase evolution in the Dongying Depression, several challenges remain to be solved. In the basins with multiple episodes of uplift and subsidence, the multi-interpretation of fluid inclusion trapping times may bring some troubles to constrain the phase evolution on the timescale. Additionally, various geological processes in a reservoir will increase the difficulty of basin modeling in reconstructing fluid phase evolution, such as crude oil cracking, gas invasion, TSR, and biodegradation. In this study, oil and gas reservoirs are adjacent to the source rocks. Hence, the compositional change after a long-distance migration through faults or sand bodies was not evaluated.

CRediT authorship contribution statement

Wenzhi Lei: Writing – original draft, Software, Methodology, Investigation, Formal analysis. **Dongxia Chen:** Writing – review & editing, Supervision, Resources, Project administration, Funding acquisition. **Ming Cheng:** Visualization, Software, Formal analysis. **Chenyang Cai:** Visualization, Formal analysis. **Qiaochu Wang:** Writing – review & editing, Methodology, Formal analysis.

Declaration of competing interest

The authors declare that they have no known competing financial interests or personal relationships that could have appeared to influence the work reported in this paper.

Acknowledgments

We appreciate the National Natural Science Foundation of China (Grant No. 41972124). We are grateful for the sample and experimental data support provided by the Sinopec Shengli Oilfield. Many thanks to the anonymous reviewers for their constructive comments, which greatly improved the quality of the manuscript. Thanks to John Stainforth for his valuable insights on basin modeling.

Data availability

Data will be made available on request.

References

Abrams, M.A., 2005. Significance of hydrocarbon seepage relative to petroleum generation and entrapment. Mar. Petrol. Geol. 22 (4), 457–477.
Aplin, A.C., Macleod, G., Larter, S.R., Pedersen, K.S., Sorensen, H., Booth, T., 1990. Combined use of Confocal Laser Scanning Microscopyand PVT simulation for estimating the composition and physical properties of petroleum in fluid inclusions. Mar. Petrol. Geol. 16 (2), 97–110.
Atlas, R.M., Hazen, T.C., 2011. Oil biodegradation and bioremediation: a tale of the two worst spills in US history. Environ. Sci. Technol. 45 (16), 6709–6715.
Baur, F., Di Primio, R., Lampe, C., Littke, R., 2011. Mass balance calculations for different models of hydrocarbon migration in the Jeanne d'Arc basin, offshore Newfoundland. J. Petrol. Geol. 34 (2), 181–198.
Bo, D., 2008. The Division and Evaluation of Hydrocarbon Accumulation System in Minfeng Area of Dongying Depression. Qingdao: China University of Petroleum (East China). (in Chinese with English abstract).
Chen, C., Wang, Y., Beagle, J.R., Liao, L., Shi, S., Deng, R., 2019. Reconstruction of the evolution of deep fluids in light oil reservoirs in the Central Tarim Basin by using PVT simulation and basin modeling. Mar. Petrol. Geol. 107, 116–126.
Claypool, G.E., Mancini, E.A., 1989. Geochemical relationships of petroleum in Mesozoic reservoirs to carbonate source rocks of Jurassic Smackover Formation, southwestern Alabama. AAPG Bull. 73 (7), 904–924.
Danesh, A., 1998. PVT and Phase Behaviour of Petroleum Reservoir Fluids. Elsevier.
Del Bianco, A., Panariti, N., Anelli, M., Beltrame, P.L., Carniti, P., 1993. Thermal cracking of petroleum residues: 1. Kinetic analysis of the reaction. Fuel 72 (1), 75–80.
Di Primio, R., Dieckmann, V., Mills, N., 1998. PVT and phase behaviour analysis in petroleum exploration. Org. Geochem. 29 (1–3), 207–222.
Di Primio, R., Horsfield, B., 2006. From petroleum-type organofacies to hydrocarbon phase prediction. AAPG (Am. Assoc. Pet. Geol.) Bull. 90 (7), 1031–1058. https://doi.org/10.1306/02140605129.
Fu, D., Zhou, S., Ma, Y., Li, J., Xu, G., Tian, T., Yang, F., 2019. Petroleum accumulation history of Nanbaxian belt—study of gas generation and fluid phase, northern margin of Qaidam Basin, West of China. J. Petrol. Sci. Eng. 178, 449–458.
Fu, M., Liu, F., Deng, H., Huang, T., Wang, H., 2015. Hydrocarbon charging period of cretaceous reservoirs in AHDEB oil field: evidence from fluid inclusion. Earth Sci. 40 (7), 1187–1196. https://doi.org/10.3799/dqkx.2015.099 (in Chinese with English abstract).
George, S.C., Ruble, T.E., Dutkiewicz, A., Eadington, P.J., 2001. Assessing the maturity of oil trapped in fluid inclusions using molecular geochemistry data and visually-determined fluorescence colours. Appl. Geochem. 16 (4), 451–473.
Goldstein, R.H., 2001. Fluid inclusions in sedimentary and diagenetic systems. Lithos 55 (1–4), 159–193.
Goldstein, R.H., Reynolds, T.J., 1994. Systematics of Fluid Inclusions in Diagenetic Minerals. SEPM Society for Sedimentary Geology.
Guo, X., Chen, J., Yuan, S., He, S., Zhao, J., 2020. Constraint of in-situ calcite U-Pb dating by laser ablation on geochronology of hydrocarbon accumulation in petroliferous basins: a case study of Dongying sag in the Bohai Bay Basin. Acta Pet. Sin. 41 (3), 284–291 (in Chinese with English abstract).
Guo, X., Liu, K., He, S., Song, G., Wang, Y., Hao, X., Wang, B., 2012. Petroleum generation and charge history of the northern Dongying Depression, Bohai Bay Basin, China: insight from integrated fluid inclusion analysis and basin modelling. Mar. Petrol. Geol. 32 (1), 21–35.
Hagemann, H.W., Hollerbach, A., 1986. The fluorescence behaviour of crude oils with respect to their thermal maturation and degradation. Org. Geochem. 10 (1–3), 473–480.
Haji-Savameri, M., Menad, N.A., Norouzi-Apourvari, S., et al., 2020. Modeling dew point pressure of gas condensate reservoirs: comparison of hybrid soft computing approaches, correlations, and thermodynamic models. J. Petrol. Sci. Eng. 184, 106558.
Hantschel, T., Kauerauf, A.I., 2009. Fundamentals of Basin and Petroleum Systems Modeling. Springer Science & Business Media.
Hao, M., Zhang, J., Li, M., Liu, L., Hao, R., 2023. Quantitative evaluation of fault transport difference and its application in tight oil and gas reservoir exploration. Petroleum Geology and Recovery Efficiency 30 (1), 60–68 (in Chinese with English abstract).
Harrison, C., Sullivan, M., Smythe, E.E.J., et al., 2022. Development of a downhole measurement system for phase behavior of reservoir crude oils and retrograde condensates. Energy Fuels 36 (16), 8624–8638.
Hill, R.J., Tang, Y., Kaplan, I.R., 2003. Insights into oil cracking based on laboratory experiments. Org. Geochem. 34 (12), 1651–1672.
Horsfield, B., 1992. Closed-system programmed-temperature pyrolysis for simulating the conversion of oil to gas in a deep petroleum reservoir. Org. Geochem. 19, 191–204.
Hunt, J.M., 1990. Generation and migration of petroleum from abnormally pressured fluid compartments. AAPG Bull. 74 (1), 1–12.
Igwe, U., Khishvand, M., Piri, M., 2022. Retrograde condensation in natural porous media: an in situ experimental investigation. Phys. Fluids 34 (1), 013102.
Jia, H., Ji, H., Wu, Z., Li, W., Zhang, H., Wang, Z., 2013. Sedimentary system and provenance orientation of the red-bed sedimentary period in Dongying Sag. Geoscience 27 (5), 1058 (in Chinese with English abstract).

Kamali, M.Z., Davoodi, S., Ghorbani, H., Wood, D.A., Mohamadian, N., Lajmorak, S., Rukavishnikov, V.S., Taherizade, F., Band, S.S., 2022. Permeability prediction of heterogeneous carbonate gas condensate reservoirs applying group method of data handling. Mar. Petrol. Geol. 139, 105597.
Kauerauf, A.I., Hantschel, T., 2009. Fundamentals of Basin and Petroleum Systems Modeling. Springer, Berlin, Heidelberg.
Krouse, H.R., Viau, C.A., Eliuk, L.S., Ueda, A., Halas, S., 1988. Chemical and isotopic evidence of thermochemical sulphate reduction by light hydrocarbon gases in deep carbonate reservoirs. Nature 333 (6172), 415–419.
Kuske, S., Horsfield, B., Jweda, J., Michael, G.E., Song, Y., 2019. Geochemical factors controlling the phase behavior of Eagle Ford Shale petroleum fluids. AAPG (Am. Assoc. Pet. Geol.) Bull. 103 (4), 835–870.
Lafargue, E., Barker, C., 1988. Effect of water washing on crude oil compositions. AAPG Bull. 72 (3), 263–276.
Lei, W., Chen, D., Wang, Y., Gong, J., Qiu, Y., Wang, Q., Ming, C., Cai, C., 2024. Accumulation mechanism and model of multi-type deep coarse-grained siliciclastic reservoirs in the eastern Jiyang Depression, Bohai Bay Basin. Oil Gas Geol. 45 (1), 113–129. https://doi.org/10.11743/ogg20240108.
Li, Y., Song, G., Li, W., Guo, R., Yang, X., Chen, C., Luo, W., 2010. A fossil oil-reservoir and the gas origin in the lower sha-4 member of the well fengshen-1 area, the north dongying zone of the Jiyang depression. Oil Gas Geol. 31 (2), 173–179. https://doi.org/10.11743/ogg20100206 (in Chinese with English abstract).
Liu, H., 2022. Geological particularity and exploration practice of Paleogene shale oil in Jiyang depression: a case study of the upper submember of Member 4 to the lower submember of Member 3 of Shahejie Formation. Acta Pet. Sin. 43 (5), 581 (in Chinese with English abstract).
Liu, H., Jiang, Y., Xu, H., Song, G., Cai, D., 2012. Genetic types and accumulation model of the deep cracked gas pools of Minfeng area in Dongying Sag. J. Jilin Univ. (Earth Sci. Ed.) 42 (6), 1638–1646 (in Chinese with English abstract).
Mello, U.T., Karner, G.D., Anderson, R.N., 1995. Role of salt in restraining the maturation of subsalt source rocks. Mar. Petrol. Geol. 12 (7), 697–716.
Milkov, A.V., 2010. Methanogenic biodegradation of petroleum in the West Siberian Basin (Russia): significance for formation of giant Cenomanian gas pools. AAPG Bull. 94 (10), 1485–1541.
Novikov, D.A., 2022. Equilibrium modeling of water-gas systems in Jurassic–Cretaceous reservoirs of the Arctic petroleum province, northern West Siberia. Petrol. Explor. Dev. 49 (2), 363–373.
Peters, K.E., Schenk, O., Hosford Scheirer, A., Wygrala, B., Hantschel, T., 2017. Basin and Petroleum System Modeling. Springer handbook of petroleum technology, pp. 381–417.
Peters, K.E., Walters, C.C., Moldowan, J.M., 2005. The Biomarker Guide. Cambridge University Press.
Ping, H., Chen, H., Jia, G., 2017. Petroleum accumulation in the deeply buried reservoirs in the northern Dongying Depression, Bohai Bay Basin, China: new insights from fluid inclusions, natural gas geochemistry, and 1-D basin modeling. Mar. Petrol. Geol. 80, 70–93.
Ping, H., Chen, H., Song, G., Liu, H., 2012. Accumulation history of the deeply buried condensate reservoir in Minfeng sag of the northern Dongying depression and its exploration significance. Acta Pet. Sin. 33 (6), 970–977.
Ping, H., Chen, H., Thiéry, R., Zhang, H., Li, P., Wu, N., 2014. Effects of oil cracking on homogenization temperature and trapping pressure of oil inclusion and its geological significance. Earth Sci. 39 (5), 587–600. https://doi.org/10.3799/dqkx.2014.056 (in Chinese with English abstract).
Pironon, J., Canals, M., Dubessy, J., Walgenwitz, F., Laplace-Builhe, C., 1998. Volumetric reconstruction of individual oil inclusions by confocal scanning laser microscopy. Eur. J. Mineral 10 (6), 1143–1150.
Qiao, R., Chen, Z., 2022. Petroleum phase evolution at high temperature: a combined study of oil cracking experiment and deep oil in Dongying Depression, eastern China. Fuel 326, 124978.
Qiao, R., Chen, Z., Li, C., Wang, D., Gao, Y., Liu, J., 2022. Petroleum phase states and accumulation models of the deep Shahejie Formation of Paleogene in dongying depression, China. J. Earth Sci. Environ. 44 (3), 374–390.
Shi, B., Wang, Z., Zhang, Z., et al., 2022. A state of the art review on the wellbore blockage of condensate gas wells: towards understanding the blockage type, mechanism, and treatment. Lithosphere 2022 (Special 12), 8076631.
Soave, G., 1972. Equilibrium constants from a modified Redlich-Kwong equation of state. Chem. Eng. Sci. 27 (6), 1197–1203.
Song, M., Wang, H., Zhang, Y., 2019. "Extrusion, tension and strike-slip" mountainforming mechanism and reservoir type of buried hills in Jiyang Depression. Editorial Department of Petroleum Geology and Recovery Efficiency 26 (4), 1–8 (in Chinese with English abstract).
Song, M., Wang, Y., Hao, X., An, T., 2021. Petroleum systems and exploration potential in deep Paleogene of the dongying saq, Bohai Bay basin. Oil Gas Geol. 42 (6), 1243–1254 (in Chinese with English abstract).
Stainforth, J.G., Reinders, J.E.A., 1990. Primary migration of hydrocarbons by diffusion through organic matter networks, and its effect on oil and gas generation. Org. Geochem. 16 (1–3), 61–74.
Stasiuk, L.D., Snowdon, L.R., 1997. Fluorescence micro-spectrometry of synthetic and natural hydrocarbon fluid inclusions:crude oil chemistry, density and application to petroleum migration. Appl. Geochem. 12 (3), 229–241.
Su, A., Chen, H., Zhao, J., Zhang, T., Feng, Y., Wang, C., 2020. Natural gas washing induces condensate formation from coal measures in the Pinghu Slope Belt of the Xihu Depression, East China Sea Basin: insights from fluid inclusion, geochemistry, and rock gold-tube pyrolysis. Mar. Petrol. Geol. 118, 104450.
Sun, J., Liang, T., Lin, X., Wang, Y., Zhang, Z., Zou, Y., 2019. Oil generation and retention kinetics from the upper Es4 source rock in the Dongying Depression. Geochimica 48 (4), 370–377 (in Chinese with English abstract).
Sweeney, J.J., Burnham, A.K., 1990. Evaluation of a simple model of vitrinite reflectance based on chemical kinetics. AAPG Bull. 74 (10), 1559–1570.
Thiéry, R., Pironon, J., Walgenwitz, F., Montel, F., 2002. Individual characterization of petroleum fluid inclusions (composition and P–T trapping conditions) by microthermometry and confocal laser scanning microscopy: inferences from applied thermodynamics of oils. Mar. Petrol. Geol. 19 (7), 847–859.
Thompson, K.F.M., 1988. Gas-condensate migration and oil fractionation in deltaic systems. Mar. Petrol. Geol. 5 (3), 237–246.
Thompson, K.F.M., 2010. Aspects of petroleum basin evolution due to gas advection and evaporative fractionation. Org. Geochem. 41 (4), 370–385.
Thompson, K.F.M., Kennicutt, M.C., Brooks, J.M., 1990. Classification of offshore Gulf of Mexico oils and gas condensates. AAPG Bull. 74 (2), 187–198.
Tissot, B.P., Welte, D.H., 1984. Petroleum Formation and Occurrence. Springer, Berlin, Heidelberg.
Ungerer, P., Behar, F., Villalba, M., Heum, O.R., Audibert, A., 1988. Kinetic modelling of oil cracking. Org. Geochem. 13 (4–6), 857–868.
Ungerer, P., Burrus, J., Doligez, B., Chénet, B.Y., Bessis, F., 1990. Basin evaluation by integrated two-dimensional modeling of heat transfer, fluid flow, hydrocarbon generation, and migration. AAPG Bull. 74 (3), 309–335.
Van Duuren, B.L., 1960. The fluorescence spectra of aromatic hydrocarbons and heterocyclic aromatic compounds. Anal. Chem. 32 (11), 1436–1442.
Volk, H., George, S.C., 2019. Using petroleum inclusions to trace petroleum systems-A review. Org. Geochem. 129, 99–123.
Wang, J., Peng, J., Cao, Y., 2022. Mid-late Eocene paleoclimate characteristics and significance in the Dongying Depression: an example from well HK1. Acta Sedimentol. Sin. 40 (4), 1059–1072 (in Chinese with English abstract).
Wang, M., Ma, R., Li, J., Lu, S., Li, C., Guo, Z., Li, Z., 2019. Occurrence mechanism of lacustrine shale oil in the Paleogene Shahejie Formation of Jiyang depression, Bohai Bay basin, China. Petrol. Explor. Dev. 46 (4), 833–846.
Wang, Y., Gong, J., Chen, D., Qiu, Y., Mao, S., Lei, W., 2023. Phase evolution and accumulation mode of hydrocarbons in deep coarse-grained clastic reservoirs in the Yanjia area, Dongying Sag, Bohai Bay Basin. Oil Gas Geol. 44 (5), 1159–1172.
Xiong, W., Zhu, J., Shi, Y., Yang, X., Zhen, Y., Zhai, P., 2019. Density distribution of crude oil in the Zhuyi depression of Pearl River Mouth Basin and control factors. Marine Geology Frontiers 35 (1), 43–52. https://doi.org/10.16028/j.1009-2722.2019.01005 (in Chinese with English abstract).
Yang, H., Zhang, P., Qiu, Y., Gong, J., Han, T., 2023. Deep self-source type hydrocarbon accumulation pattern and exploration practice in Dongying Sag. China Petroleum Exploration 28 (2), 92–101.
Yao, Y., Xu, D., Zhang, H., Han, Y., Zhang, S., Yin, Z., Li, B., He, Q., Bian, X., 2007. A brief introduction to the cenozoic astrostratigraphic time scale for the Dongying Depression, Shangdong. J. Stratigr. (S2), 423–429 (in Chinese with English abstract).
Zhang, S., Huang, H., Su, J., Liu, M., 2015. Ultra-deep liquid hydrocarbon exploration potential in cratonic region of the Tarim Basin inferred from gas condensate genesis. Fuel 160, 583–595.
Zhang, Z., Zhang, Y., Zhu, G., Chi, L., Han, J., 2019. Impacts of thermochemical sulfate reduction, oil cracking, and gas mixing on the petroleum fluid phase in the Tazhong area, Tarim Basin, China. Energy Fuels 33 (2), 968–978.
Zhu, G., Zhang, B., Yang, H., Su, J., Liu, K., Zhu, Y., 2014. Secondary alteration to ancient oil reservoirs by late gas filling in the Tazhong area, Tarim Basin. J. Petrol. Sci. Eng. 122, 240–256.
Zhu, G., Zhang, S., Huang, H., Liang, Y., Meng, S., Li, Y., 2011. Gas genetic type and origin of hydrogen sulfide in the Zhongba gas field of the western Sichuan Basin, China. Appl. Geochem. 26 (7), 1261–1273.